Production of η and η' mesons in pp and pPb collisions

R. Aaij *et al.*[*]
(LHCb Collaboration)

(Received 27 October 2023; accepted 22 January 2024; published 13 February 2024)

The production of η and η' mesons is studied in proton-proton and proton-lead collisions collected with the LHCb detector. Proton-proton collisions are studied at center-of-mass energies of 5.02 and 13 TeV and proton-lead collisions are studied at a center-of-mass energy per nucleon of 8.16 TeV. The studies are performed in center-of-mass (c.m.) rapidity regions $2.5 < y_{\text{c.m.}} < 3.5$ (forward rapidity) and $-4.0 < y_{\text{c.m.}} < -3.0$ (backward rapidity) defined relative to the proton beam direction. The η and η' production cross sections are measured differentially as a function of transverse momentum for $1.5 < p_{\text{T}} < 10$ GeV and $3 < p_{\text{T}} < 10$ GeV, respectively. The differential cross sections are used to calculate nuclear modification factors. The nuclear modification factors for η and η' mesons agree at both forward and backward rapidity, showing no significant evidence of mass dependence. The differential cross sections of η mesons are also used to calculate η/π^0 cross-section ratios, which show evidence of a deviation from the world average. These studies offer new constraints on mass-dependent nuclear effects in heavy-ion collisions, as well as η and η' meson fragmentation.

DOI: 10.1103/PhysRevC.109.024907

I. INTRODUCTION

Light hadron production in heavy-ion collisions is a sensitive probe of the structure of the colliding nuclei. Pion production data from deuteron-gold (d-Au) collisions at the BNL Relativistic Heavy Ion Collider (RHIC) have been used to constrain nuclear parton distribution functions (nPDFs) [1–5]. These nPDFs encode modifications of the partonic structure of nuclei within the collinear factorization framework [6]. In addition, light hadron production is also sensitive to effects of the high energy densities produced in heavy-ion collisions. Light hadron production was one of the original tools used to study quark-gluon plasma (QGP) in heavy-ion collisions. Measurements of angular correlations between light hadrons in heavy-ion collisions at RHIC demonstrated collective flow and were interpreted as some of the first evidence for QGP production [7–10]. Similar correlations have been observed in small-collision systems at the Large Hadron Collider (LHC) and RHIC, pointing to possible QGP formation [11–17].

Nuclear effects on particle production can be quantified using the nuclear modification factor, which is defined as

$$R_{p\text{Pb}} = \frac{1}{A}\frac{d\sigma_{p\text{Pb}}/dp_{\text{T}}}{d\sigma_{pp}/dp_{\text{T}}}, \tag{1}$$

where $A = 208$ is the atomic mass of the lead nucleus, while $d\sigma_{p\text{Pb}}/dp_{\text{T}}$ and $d\sigma_{pp}/dp_{\text{T}}$ are the differential cross sections as a function of transverse momentum p_{T} in pPb and pp collisions, respectively. The LHCb experiment recently measured the nuclear modification factors of inclusive charged particles in proton-lead (pPb) collisions at $\sqrt{s_{\text{NN}}} = 5.02$ TeV and π^0 meson production at 8.16 TeV, observing enhancements in the lead-going direction larger than those predicted by nPDF calculations [18,19]. These enhancements could be produced by effects such as hydrodynamic evolution of QGP created in these collisions [20]. Understanding the origin of QGP-like effects in small collision systems is one of the primary goals of high-energy nuclear physics.

Studying the production of π^0, η, and η' mesons in heavy-ion collisions allows for the isolation of the mass and isospin dependence of nuclear effects, which can help reveal the origin of QGP-like phenomena in small-collision systems. Collective radial flow of the QGP, for example, is expected to produce larger enhancements for heavier particles, as heavier particles must receive a larger momentum boost in order to comove with an expanding medium [21,22]. Studies of the multiplicity dependence of identified particle production in proton-proton (pp) collisions by the ALICE Collaboration indicate a hardening of the p_{T} spectra with increasing multiplicity that is more pronounced for baryons and strange mesons than for pions [23,24]. The authors interpret these results as a mass ordering consistent with radial flow. This interpretation is further complicated, however, by differences in the number and flavor of valence quarks between the hadron species. The η and η' mesons have similar masses to the kaon and proton, respectively, but with different valence quark content. As a result, studies of production of η and η' mesons can clarify the origin of these flow-like effects.

The production of η mesons has been studied extensively in small-collision systems at central rapidity at RHIC and the Large Hadron Collider (LHC) [5,25–30]. In addition, the STAR and PHENIX Collaborations have studied η meson

[*]Full author list given at the end of the article.

production at forward rapidity in polarized pp collisions at $\sqrt{s} = 200$ GeV [31,32]. There are no studies, however, of η meson production at forward or backward rapidity in collisions involving heavy ions. Furthermore, η' meson production has only been studied in pp collisions at $\sqrt{s} = 200$ GeV by the PHENIX Collaboration [25]. The η' nuclear modification factor has never been measured in heavy-ion collisions. Studying both η and η' production at forward and backward rapidities helps reveal the mass and rapidity dependence of nuclear effects in heavy-ion collisions.

This article presents measurements of η and η' meson production with the LHCb detector. The η and η' cross sections are measured differentially in $p_{\rm T}$ in pp collisions at $\sqrt{s} = 5.02$ and 13 TeV, and in pPb collisions at 8.16 TeV. The η meson cross sections are combined with previous LHCb measurements of the π^0 differential cross sections to calculate the η/π^0 cross-section ratio. Finally, the nuclear modification factors are reported as a function of $p_{\rm T}$. Since LHCb collected a relatively small sample of unbiased pp collisions at $\sqrt{s} = 8$ TeV, the pp reference cross section is constructed by interpolating between the $\sqrt{s} = 5.02$ and 13 TeV cross-section measurements. The measurements are performed in the center-of-mass (c.m.) rapidity ($y_{\rm c.m.}$) ranges $2.5 < y_{\rm c.m.} < 3.5$ and $-4.0 < y_{\rm c.m.} < -3.0$, which correspond to the overlapping portions of the pp and pPb fiducial regions. The center-of-mass rapidity is related to the laboratory-frame rapidity $y_{\rm lab}$ by $y_{\rm c.m.} = y_{\rm lab} - 0.465$ in pPb collisions and $|y_{\rm c.m.}| = y_{\rm lab}$ in pp collisions. The η meson measurements are performed for $1.5 < p_{\rm T} < 10.0$ GeV, while the η' meson measurements are performed for $3 < p_{\rm T} < 10$ GeV (natural units are used throughout this article).

II. DETECTOR AND DATA SET

The LHCb detector is a single-arm forward spectrometer covering the pseudorapidity range $2 < \eta < 5$, described in detail in Refs. [33,34]. The detector includes a high-precision tracking system consisting of a silicon-strip vertex detector (VELO) surrounding the pp interaction region, a large-area silicon-strip detector located upstream of a dipole magnet, and three stations of silicon-strip detectors and straw drift tubes placed downstream of the magnet. Different types of charged hadrons are distinguished using information from two ring-imaging Cherenkov detectors. Photons are reconstructed and identified by a calorimeter system consisting of scintillating-pad (SPD) and preshower (PRS) detectors, an electromagnetic (ECAL), and a hadronic (HCAL) calorimeter. Muons are identified by a system composed of alternating layers of iron and multiwire proportional chambers. Particularly important for this analysis is the ECAL, which consists of alternating layers of lead and scintillator and has an energy E resolution of $13.5\%/\sqrt{E/\,\text{GeV}} \oplus 5.2\% \oplus (0.32\ \text{GeV})/E$ [35]. Simulated data samples are used to model the detector response to η and η' reconstruction. In the simulation, pPb collisions are generated using EPOS-LHC [20], while pp collisions are generated using PYTHIA [36]. Decays of unstable particles are described by EVTGEN [37], and final-state radiation is generated using PHOTOS [38]. The interaction of the generated particles with the detector, and its response, are implemented using the GEANT4 toolkit [39,40], as described in Ref. [41].

Proton-lead collisions are recorded in two configurations: the forward configuration in which the proton beam travels from the interaction region toward the spectrometer, and the backward configuration in which the lead ion beam travels toward the spectrometer. The forward configuration data are used to perform measurements for positive $y_{\rm c.m.}$, and the backward data are used for negative $y_{\rm c.m.}$. The pPb data used in this analysis were collected in 2016 and correspond to an integrated luminosity of 350 ± 9 μb^{-1} (364 ± 9 μb^{-1}) in the forward (backward) direction [42,43]. All pPb events are required to have at least one reconstructed track in the VELO. The pp data were collected in 2015 and correspond to an integrated luminosity of 3.49 ± 0.07 nb^{-1} (6.86 ± 0.14 nb^{-1}) for $\sqrt{s} = 5.02$ TeV ($\sqrt{s} = 13$ TeV).

Signal η candidates are reconstructed from pairs of photons. Photons are reconstructed from energy deposits (clusters) in the ECAL. The ECAL clusters are required to have $p_{\rm T} > 500$ MeV and must be far from the extrapolated trajectories of all reconstructed tracks to exclude clusters produced by charged particles. In addition, clusters produced by hadrons are removed using a neural network classifier that takes as input the significance of the cluster's distance to the nearest track, variables describing the ECAL and PRS cluster shapes, and energy deposited in the SPD, PRS, ECAL, and HCAL. Selected η candidates with a diphoton mass $M(\gamma\gamma)$ satisfying $500\ \text{MeV} < M(\gamma\gamma) < 600$ MeV are combined with pairs of tracks to form the η' candidates. The tracks are required to be of good quality and to be consistent with originating from the same primary collision vertex (PV). The tracks also must be identified as charged pions and have $p_{\rm T} > 400$ MeV.

III. CROSS-SECTION DETERMINATION

The differential cross section in a particular $p_{\rm T}$ interval is given by

$$\frac{d\sigma}{dp_{\rm T}} = \frac{1}{\mathcal{L}\mathcal{B}\epsilon(p_{\rm T})}\frac{N(p_{\rm T})}{\Delta p_{\rm T}}, \tag{2}$$

where $\mathcal{L}$ is the integrated luminosity of the sample, $\mathcal{B}$ is the branching ratio of the η or η' meson to the reconstructed final state, and $\epsilon(p_{\rm T})$ is a correction factor that accounts for detector inefficiencies and migration between $p_{\rm T}$ intervals due to finite detector resolution. The signal yield in a given $p_{\rm T}$ interval is denoted $N(p_{\rm T})$, and $\Delta p_{\rm T}$ is the size of the $p_{\rm T}$ interval. The η meson is studied using its decay to two photons and the η' meson is studied using its decay to $\pi^+\pi^-\eta$, which have branching fractions of $(39.36 \pm 0.18)\%$ and $(42.5 \pm 0.5)\%$, respectively [44]. The signal yields are determined using binned maximum-likelihood fits to the mass spectra of reconstructed signal candidates [45,46]. Example fit results from pPb collisions with $2.5 < y_{\rm c.m.} < 3.5$ for $1.5 < p_{\rm T} < 1.6$ GeV and $3.0 < p_{\rm T} < 3.2$ GeV are shown in Fig. 1. The η meson signal is modeled using a two-sided Crystal Ball function [47]. The parameters describing the tails of the distribution are determined from fits to simulation, which are used to impose Gaussian constraints in the fits to

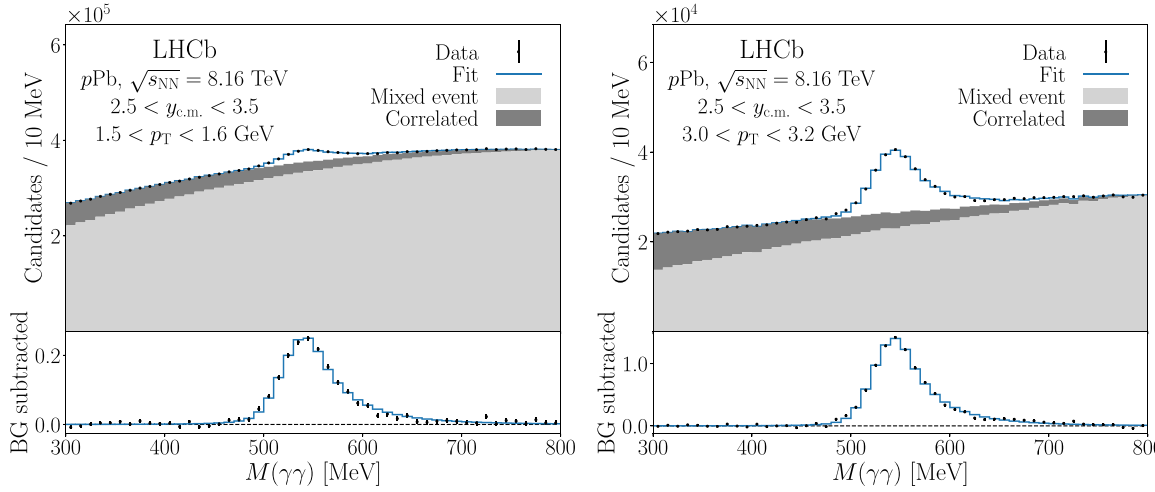

FIG. 1. Example reconstructed $M(\gamma\gamma)$ distributions in forward pPb collisions at $\sqrt{s_{NN}} = 8.16$ TeV with $2.5 < y_{c.m.} < 3.5$. Distributions are shown for (left) $1.5 < p_T < 1.6$ GeV and (right) $3.0 < p_T < 3.2$ GeV. Fit results are overlaid, including the mixed event and correlated combinatorial background templates. The lower panels show the background-subtracted mass distributions with the fit results overlaid.

data. Most of the background consists of random combinations of photons, which are modeled using an event mixing technique in which reconstructed photons from different events are combined. The mass distributions of the mixed-event photon pairs are used to create background template histograms. In addition to these uncorrelated combinations, an additional background source arises from the correlated production of photons nearby in the detector, such as the combination of two photons from the same jet. These photon pairs tend to be produced with small opening angles. As a result, the background should be largest at the low edge of the mass spectrum and monotonically decrease as a function of $M(\gamma\gamma)$. This background is therefore modeled using a function of the form

$$f(x) \propto 1 - \left(\frac{x - m_0}{m_1 - m_0}\right)^n, \tag{3}$$

where $x = M(\gamma\gamma)$, $m_0 = 300$ MeV is the low edge of the mass spectra used in the fit, $m_1 = 800$ MeV is the high edge, and n is a free parameter. This empirical function provides a good description of the correlated background in simulated samples of η meson decays.

The η' candidate mass $M(\pi^+\pi^-\eta)$ is determined using a kinematic fit with the decay vertex constrained to a PV and $M(\gamma\gamma)$ fixed to the world-average η meson mass [44]. Example fits from pPb collisions with $2.5 < y_{c.m.} < 3.5$ for $3 < p_T < 4$ GeV and $7 < p_T < 10$ GeV are shown in Fig. 2. The η' meson signal is modeled using two Gaussian functions with a common mean. The widths of the two Gaussian functions and their relative contributions to the signal peak are determined from fits to simulation. The results of fits to simulated events are used to impose Gaussian constraints in the fits to data. The uncorrelated combinatorial background is modeled using mixed-event combinations of dipion and η

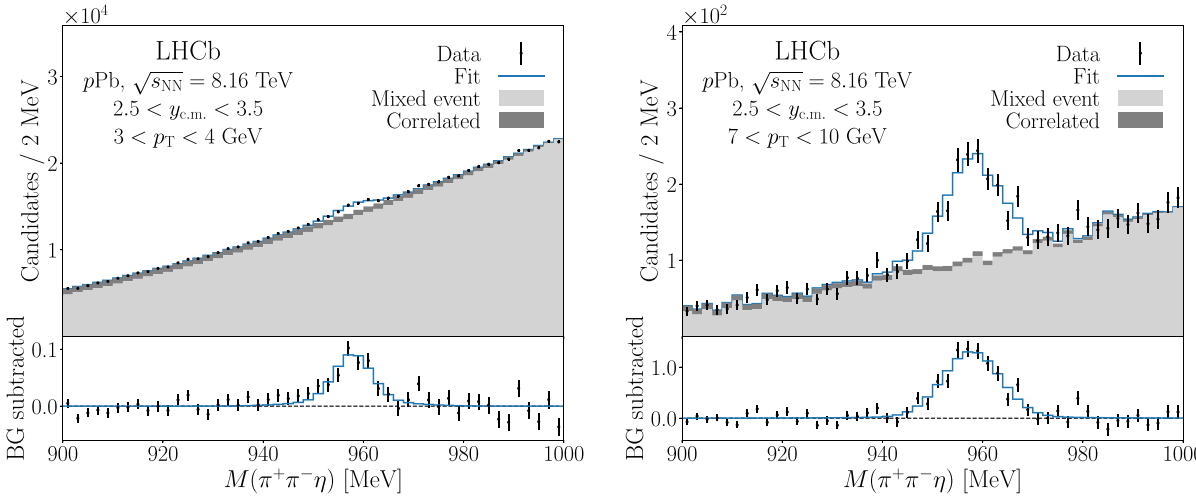

FIG. 2. Example reconstructed $M(\pi^+\pi^-\eta)$ distributions in forward pPb collisions at $\sqrt{s_{NN}} = 8.16$ TeV with $2.5 < y_{c.m.} < 3.5$. Distributions are shown for (left) $3 < p_T < 4$ GeV and (right) $7 < p_T < 10$ GeV. Fit results are overlaid, including the mixed event and correlated combinatorial background templates. The lower panels show the background-subtracted mass distributions with the fit results overlaid.

TABLE I. Relative systematic and statistical uncertainties in $d\sigma^{\eta}/dp_{\mathrm{T}}$, $R^{\eta}_{p\mathrm{Pb}}$, $d\sigma^{\eta'}/dp_{\mathrm{T}}$, and $R^{\eta'}_{p\mathrm{Pb}}$, where the superscript denotes the hadron species. The uncertainties are reported in percent, and the ranges correspond to the minimum and maximum values of the associated uncertainties across all p_{T} intervals, $y_{\mathrm{c.m.}}$ regions, and datasets. All sources of systematic uncertainty are approximately fully correlated across p_{T} intervals.

Source (%)	$d\sigma^{\eta}/dp_{\mathrm{T}}$	$R^{\eta}_{p\mathrm{Pb}}$	$d\sigma^{\eta'}/dp_{\mathrm{T}}$	$R^{\eta'}_{p\mathrm{Pb}}$
Fit model	0.7–22.9	0.5–12.3	6.0–33.8	2.5–26.4
Unfolding	0.1–2.9	0.1–2.5	0.1–0.3	0.1–0.4
Interpolation	...	0.5–7.5	...	0.1–9.1
Material budget	8.0	...	10.8	...
Photon efficiency	2.5–4.5	1.9–4.7	5.8–10.5	10.1–11.5
Tracking efficiency	...	...	0.2–0.5	0.2–0.4
Luminosity	2.0–2.6	2.2–2.3	2.0–2.6	2.2–2.3
Total systematic	9.1–24.6	3.4–14.8	16.4–36.6	10.8–29.1
Statistical	1.6–13.1	2.7–10.6	4.8–26.1	6.8–16.4

candidates. Correlated combinatorial background makes a much smaller relative contribution to the η' mass spectra than to that of the η meson and is modeled using the functional form of Eq. (3) with $x = M(\pi^+\pi^-\eta)$ with $n = 1$, $m_0 = 900$ MeV, and $m_1 = 1000$ MeV.

The signal yields are corrected for the effects of the detector response using simulation. The correction factors ϵ are determined using an iterative unfolding procedure. First, correction factors are calculated for each p_{T} interval. Hagedorn functions are then fit to the corrected p_{T} spectra in data and the true p_{T} spectra in simulation [48]. The ratio of these distributions is used to weight the true signal p_{T} spectrum in simulation so that the true p_{T} spectrum of the simulated data matches the p_{T} spectrum of the corrected data. The procedure is then repeated using the weighted simulated data sample. For the η meson spectra, the procedure consistently converges after three iterations. Since the momenta of the η' candidates are carried partially by charged particles, these candidates are reconstructed with better momentum resolution than the η candidates. Furthermore, the η' measurement is performed in p_{T} intervals that are much larger than the p_{T} resolution. Consequently, only one iteration is used to determine the η' correction factors.

The η and η' reconstruction efficiencies are calibrated using data. The ECAL cluster reconstruction efficiency is measured using a tag-and-probe method with photons that convert to an e^+e^- pair in the detector material upstream of the LHCb magnetic-field region [49]. These converted photons are reconstructed as pairs of tracks. The tag electron must be matched to a cluster in the ECAL and identified as an electron, and the cluster efficiency is the fraction of probe electrons matched to an ECAL cluster. The photon identification efficiency is studied using π^0 decays to two photons, where one photon is a converted photon. The π^0 yields are extracted using a maximum-likelihood fit to the diphoton mass spectrum following Ref. [19]. The photon identification efficiency is then the fraction of π^0 mesons for which the ECAL photon passes the photon identification criteria. The charged-pion reconstruction and identification performance is studied using a tag-and-probe method with K^0_{S} decays to $\pi^+\pi^-$ pairs.

The η and η' differential cross sections in pp collisions at 8.16 TeV are estimated by interpolating between the measured pp cross sections at $\sqrt{s} = 5.02$ and 13 TeV. The interpolation is performed independently in each p_{T} interval. The cross section is interpolated using the functional form $\sigma(\sqrt{s}) = a(\sqrt{s})^b$. This procedure is found to give the correct yields to within 1% in simulated pp collisions at $\sqrt{s} = 8.16$ TeV generated using PYTHIA . A linear interpolation in $\sqrt{s}$ is also considered and provides less accurate results in simulation.

IV. SYSTEMATIC UNCERTAINTIES

The systematic uncertainties are summarized in Table I. The largest source of systematic uncertainty for the η differential cross section in most p_{T} regions is the detector material budget. The material budget is proportional to the photon conversion probability, and uncertainties in the material budget lead to uncertainties in the photon reconstruction efficiency. The photon conversion probability has been measured with an uncertainty of 4%. This uncertainty is fully correlated between photons, resulting in a constant 8% uncertainty on the differential cross section that fully cancels in the $R_{p\mathrm{Pb}}$ measurement.

At low p_{T}, the η differential cross-section uncertainty is dominated by contributions from the mass fit model. A systematic uncertainty associated with the choice of background model is estimated by replacing the uncorrelated background model with an exponential function and taking the difference with the default fit. An uncertainty associated with the choice of signal model is estimated by extracting the yield by integrating the background-subtracted mass spectra from the default fit in the range 450 MeV $< M(\gamma\gamma) <$ 700 MeV. The difference in signal yields between the default result and the background-subtracted result is taken as the signal model uncertainty. The total fit-model uncertainty varies from greater than 20% at low p_{T} to less than around 5% for p_{T} greater than about 2 GeV. Where the fit-model uncertainty is dominant, the background model uncertainty is typically much larger than the signal model uncertainty. The fit-model uncertainty partially cancels in $R_{p\mathrm{Pb}}$.

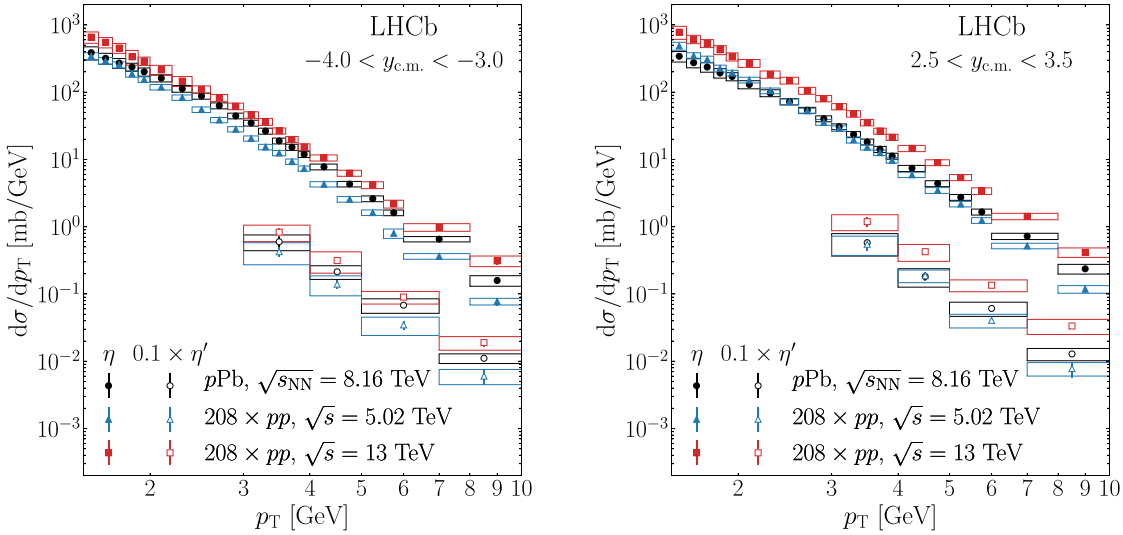

FIG. 3. Measured η and η' differential cross sections in the (left) backward and (right) forward regions. The pp cross sections are scaled by the atomic mass of the lead ion, $A = 208$. The η' cross sections are scaled down by a factor of 10 for visual clarity. Statistical uncertainties are shown as error bars, while systematic uncertainties are shown as error boxes.

An additional systematic uncertainty arises in the $R_{p\rm Pb}$ measurement due to the pp interpolation procedure. The interpolation uncertainty is estimated by repeating the procedure using a linear interpolation model, as well as a relative placement method [50]. In the relative placement procedure, placement factors are calculated using simulation assuming a linear or a power-law dependence of the cross section on $\sqrt{s}$ and then applied to data. The maximum variation of the interpolation result using these different methods is taken as the interpolation uncertainty. The resulting uncertainty varies between about 2% and 5%.

Smaller sources of uncertainty come from unfolding, the luminosity estimates, and the efficiency correction factors. The unfolding uncertainty arises from differences in the $p_{\rm T}$ resolution of the η candidates between data and simulation, as well as differences between the underlying $p_{\rm T}$ distributions. The $p_{\rm T}$ resolution differences are estimated by comparing the η signal peak widths in data and simulation, and the

TABLE II. Measured $d\sigma/dp_{\rm T}$ of η production in pp collisions at $\sqrt{s} = 5.02$ TeV. Results and uncertainties are given in mb/GeV. The first uncertainty is statistical and the second is systematic. The statistical uncertainty is uncorrelated between $p_{\rm T}$ intervals, while the systematic uncertainty is approximately fully correlated.

$p_{\rm T}$ (GeV)	$2.5 < y_{\rm c.m.} < 3.5$	$3.0 < y_{\rm c.m.} < 4.0$
1.5–1.6	$2.34 \pm 0.11 \pm 0.32$	$1.65 \pm 0.09 \pm 0.21$
1.6–1.7	$1.68 \pm 0.08 \pm 0.17$	$1.41 \pm 0.07 \pm 0.16$
1.7–1.8	$1.48 \pm 0.06 \pm 0.17$	$1.23 \pm 0.05 \pm 0.13$
1.8–1.9	$1.09 \pm 0.05 \pm 0.13$	$0.90 \pm 0.04 \pm 0.10$
1.9–2.0	$0.928 \pm 0.038 \pm 0.090$	$0.742 \pm 0.031 \pm 0.069$
2.0–2.2	$0.731 \pm 0.021 \pm 0.071$	$0.572 \pm 0.017 \pm 0.053$
2.2–2.4	$0.505 \pm 0.015 \pm 0.049$	$0.400 \pm 0.012 \pm 0.037$
2.4–2.6	$0.348 \pm 0.011 \pm 0.033$	$0.265 \pm 0.008 \pm 0.025$
2.6–2.8	$0.254 \pm 0.008 \pm 0.023$	$0.186 \pm 0.006 \pm 0.017$
2.8–3.0	$0.172 \pm 0.007 \pm 0.017$	$0.136 \pm 0.005 \pm 0.012$
3.0–3.2	$0.139 \pm 0.005 \pm 0.013$	$(9.87 \pm 0.36 \pm 0.89) \times 10^{-2}$
3.2–3.4	$(9.42 \pm 0.39 \pm 0.99) \times 10^{-2}$	$(7.38 \pm 0.32 \pm 0.69) \times 10^{-2}$
3.4–3.6	$(7.33 \pm 0.29 \pm 0.67) \times 10^{-2}$	$(6.00 \pm 0.24 \pm 0.54) \times 10^{-2}$
3.6–3.8	$(6.06 \pm 0.25 \pm 0.55) \times 10^{-2}$	$(4.47 \pm 0.19 \pm 0.41) \times 10^{-2}$
3.8–4.0	$(4.67 \pm 0.24 \pm 0.43) \times 10^{-2}$	$(3.53 \pm 0.19 \pm 0.32) \times 10^{-2}$
4.0–4.5	$(2.84 \pm 0.11 \pm 0.26) \times 10^{-2}$	$(2.06 \pm 0.08 \pm 0.19) \times 10^{-2}$
4.5–5.0	$(1.67 \pm 0.08 \pm 0.16) \times 10^{-2}$	$(1.23 \pm 0.06 \pm 0.12) \times 10^{-2}$
5.0–5.5	$(1.05 \pm 0.06 \pm 0.10) \times 10^{-2}$	$(7.80 \pm 0.43 \pm 0.74) \times 10^{-3}$
5.5–6.0	$(5.97 \pm 0.61 \pm 0.58) \times 10^{-3}$	$(3.84 \pm 0.29 \pm 0.61) \times 10^{-3}$
6.0–8.0	$(2.49 \pm 0.13 \pm 0.24) \times 10^{-3}$	$(1.75 \pm 0.11 \pm 0.17) \times 10^{-3}$
8.0–10.0	$(5.67 \pm 0.67 \pm 0.74) \times 10^{-4}$	$(3.72 \pm 0.49 \pm 0.42) \times 10^{-4}$

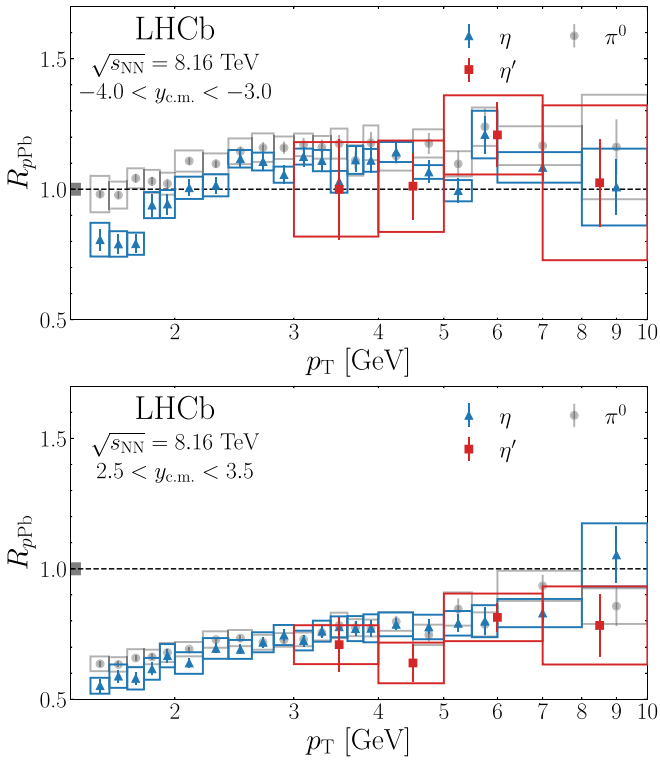

FIG. 4. Measured η and η' nuclear modification factors in the (top) backward and (bottom) forward regions. Error bars show the statistical uncertainties, while the boxes show the systematic uncertainties except for the uncertainty associated with the luminosity, which is fully correlated between measurements. The luminosity uncertainty is shown as a dark gray shaded box. The η and η' results are compared with the π^0 data from Ref. [19].

resolution is varied in the unfolding accordingly. The effect of differences in the underlying $p_{\rm T}$ distribution is estimated by weighting the simulated data to vary the initial $p_{\rm T}$ distribution. The resulting systematic uncertainty is around 1% or less in every $p_{\rm T}$ interval. The efficiency correction uncertainty arises from the finite size of the simulated data samples and results in global uncertainties of about 1%–2%. The luminosity has been measured in pp collisions with a precision of 2% and in pPb collisions with a precision of 2.6% in the forward configuration and 2.5% in the backward configuration [43]. The luminosity uncertainty is 50% correlated between datasets.

The fit model is the dominant source of uncertainty in the η'-related measurements in most $p_{\rm T}$ intervals. The background model uncertainty is estimated by repeating the fit using a polynomial function to model the background and taking the difference with the default result. The signal model uncertainty is estimated by integrating the background-subtracted mass spectrum between 940 and 980 MeV and taking the difference with the default fit result. The resulting total uncertainty varies between 6% and about 34%. This uncertainty partially cancels in $R_{p\rm Pb}$, resulting in uncertainties of about 3%–26%. The next largest source of uncertainty is the material budget. The material budget uncertainty is the same as for the η measurement, with an additional 1.4% uncertainty per charged pion in the final state. The resulting total uncertainty is 10.8% across the full $p_{\rm T}$ range. This uncertainty fully cancels in the $R_{p\rm Pb}$ measurement. The photon reconstruction and identification correction uncertainty is about 6%–10%. Uncertainties associated with the track reconstruction and particle identification efficiencies are determined by varying the tracking efficiency calibration factors according to their uncertainties. The resulting uncertainty is less than 1% in every $p_{\rm T}$ interval. Additional uncertainties come from the luminosity determination, unfolding, and interpolation. These sources of uncertainty are estimated using the same methods used for the η measurements and are subdominant.

V. RESULTS

The measured η and η' differential cross sections are shown in Fig. 3. Results for the η meson are tabulated in Tables II–IV (these and subsequent tables are in the Appendix), and

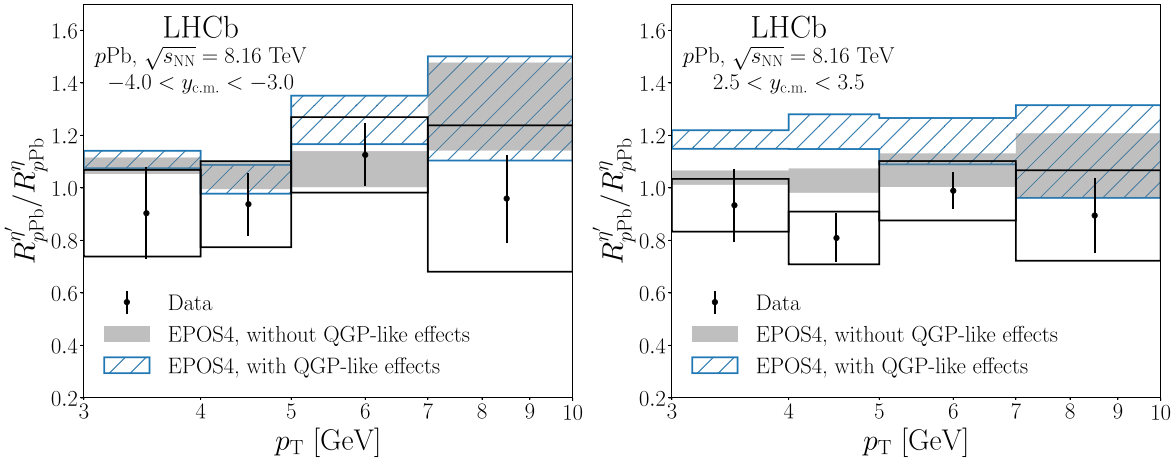

FIG. 5. Measured $R^{\eta'}_{p\rm Pb}/R^{\eta}_{p\rm Pb}$ in the (left) backward and (right) forward regions. Error bars show the statistical uncertainties, while the boxes show the systematic uncertainties. The systematic uncertainties are approximately fully correlated in $p_{\rm T}$. The results are compared with predictions from EPOS4 with and without QGP-like effects. The shaded and hatched regions show the statistical 68% confidence-level regions of the predictions.

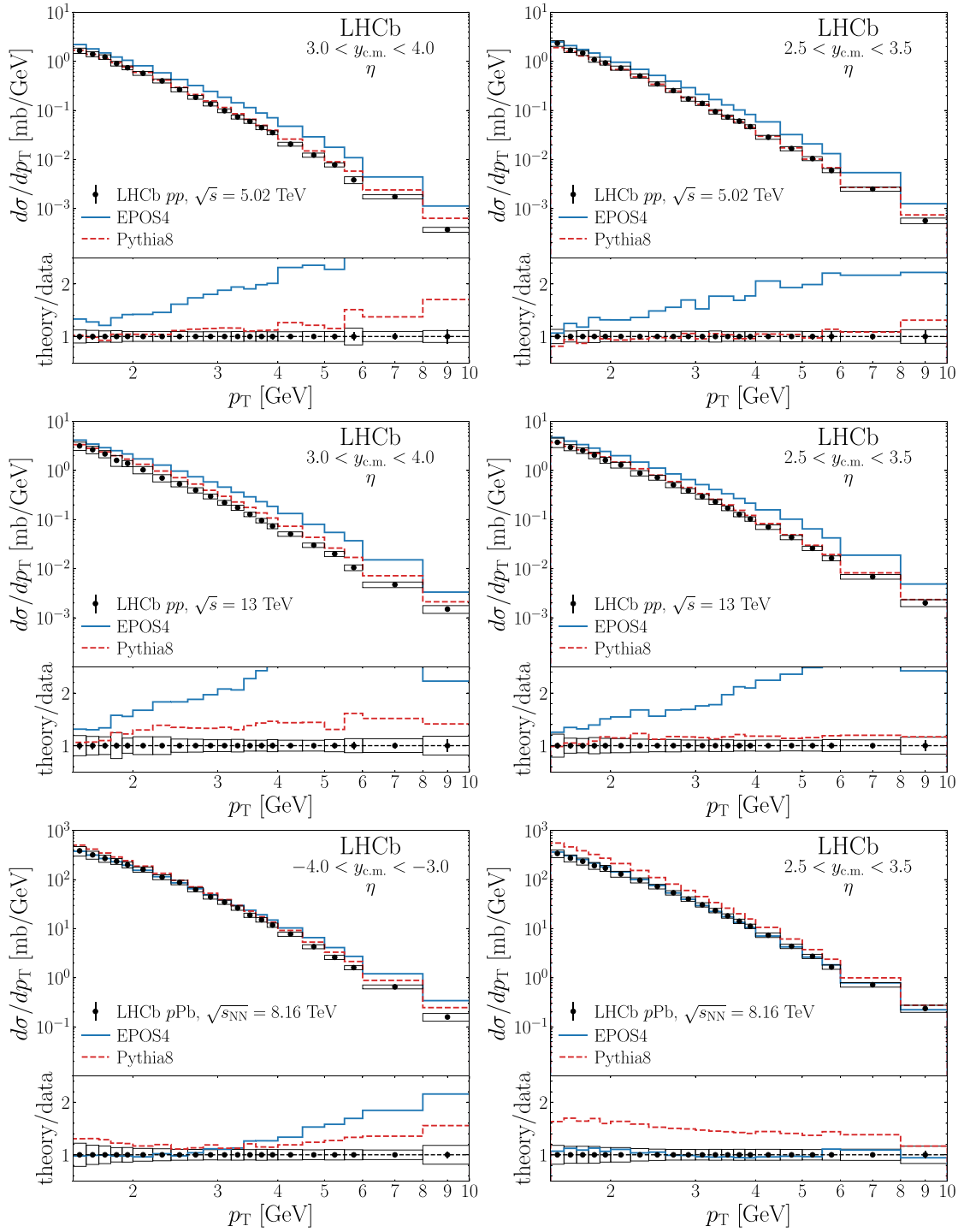

FIG. 6. Measured η differential cross sections in the (left) backward and (right) forward regions. Results are shown for pp collisions at (top) $\sqrt{s} = 5.02$ and (middle) 13 TeV and (bottom) for pPb collisions at $\sqrt{s_{NN}} = 8.16$ TeV. Results are compared with predictions from EPOS4 and PYTHIA8. The lower panels show the ratios of the predictions to the measured results. The statistical uncertainties are shown by error bars, while systematic uncertainties are shown by boxes.

the results for the η' meson are tabulated in Tables V–VII. The differential cross sections are used to calculate nuclear modification factors, which are shown in Fig. 4 and tabulated in Tables VIII and IX. In the forward region, the η, π^0, and η' results all agree where their fiducial regions overlap. The observed suppression is consistent with the effects of nuclear shadowing of the gluon density seen in global nPDF analyses [51–53]. In the backward region, the π^0 and η measurements deviate at low p_T and converge for $p_T > 3$ GeV. In this region, the π^0, η, and η' measurements

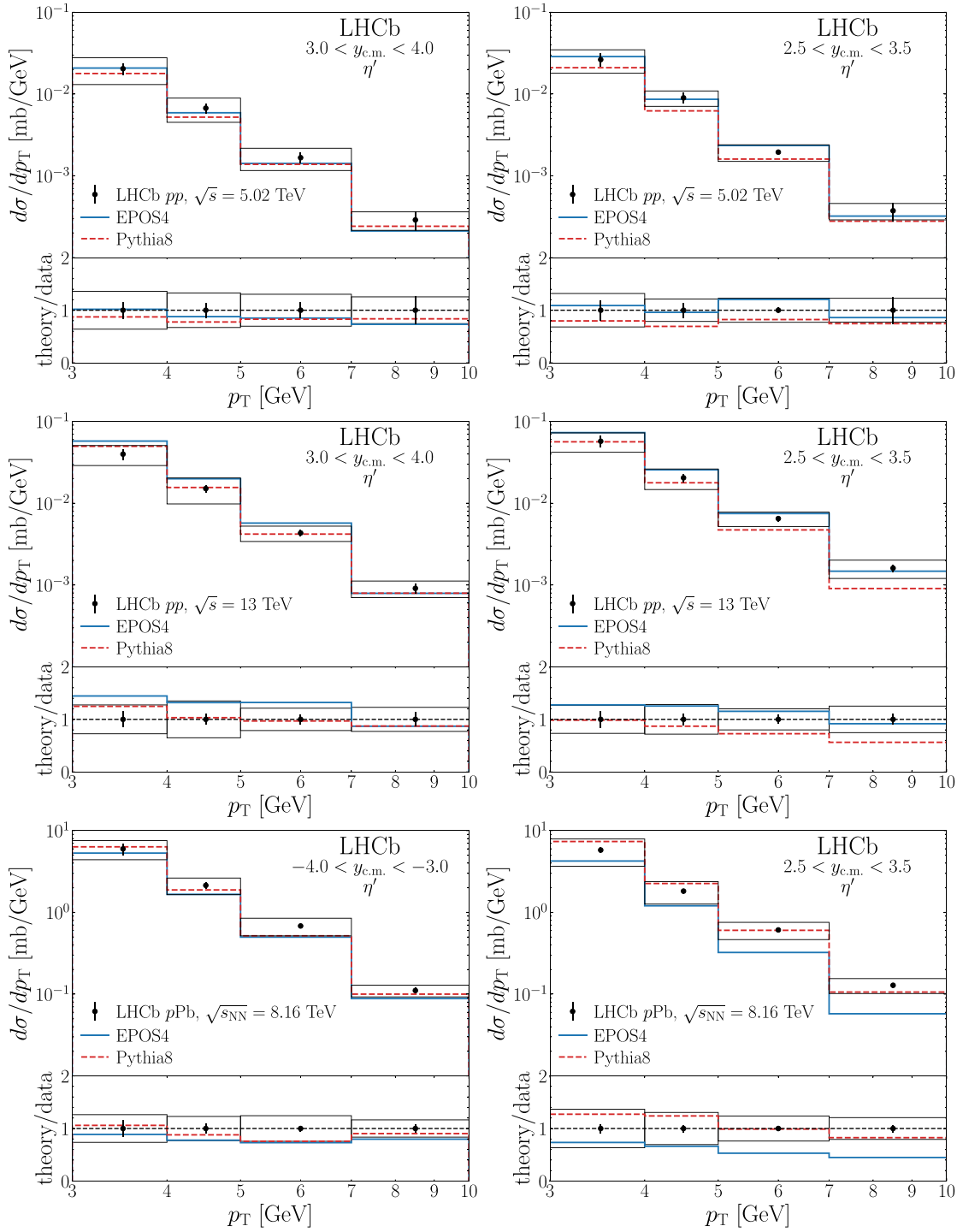

FIG. 7. Measured η' differential cross sections in the (left) backward and (right) forward regions. Results are shown for pp collisions at (top) $\sqrt{s} = 5.02$ and (middle) 13 TeV and (bottom) for pPb collisions at $\sqrt{s_{NN}} = 8.16$ TeV. Results are compared with predictions from EPOS4 and PYTHIA8. The lower panels show the ratios of the predictions to the measured results. The statistical uncertainties are shown by error bars, while systematic uncertainties are shown by boxes.

all agree. The results show no significant evidence for mass dependence of the nuclear modification factor of light neutral mesons.

The measured nuclear modification factor ratio $R^{\eta'}_{p\mathrm{Pb}}/R^{\eta}_{p\mathrm{Pb}}$, where the superscript denotes the meson species of the nuclear modification factor, is shown in Fig. 5. Since the $R^{\eta'}_{p\mathrm{Pb}}$ and $R^{\eta}_{p\mathrm{Pb}}$ measurements are performed in different p_T regions, the denominator of the ratio of nuclear modification factors is constructed by fitting $R^{\eta}_{p\mathrm{Pb}}$ using a Gaussian process regression [54]. A systematic uncertainty is obtained by repeating

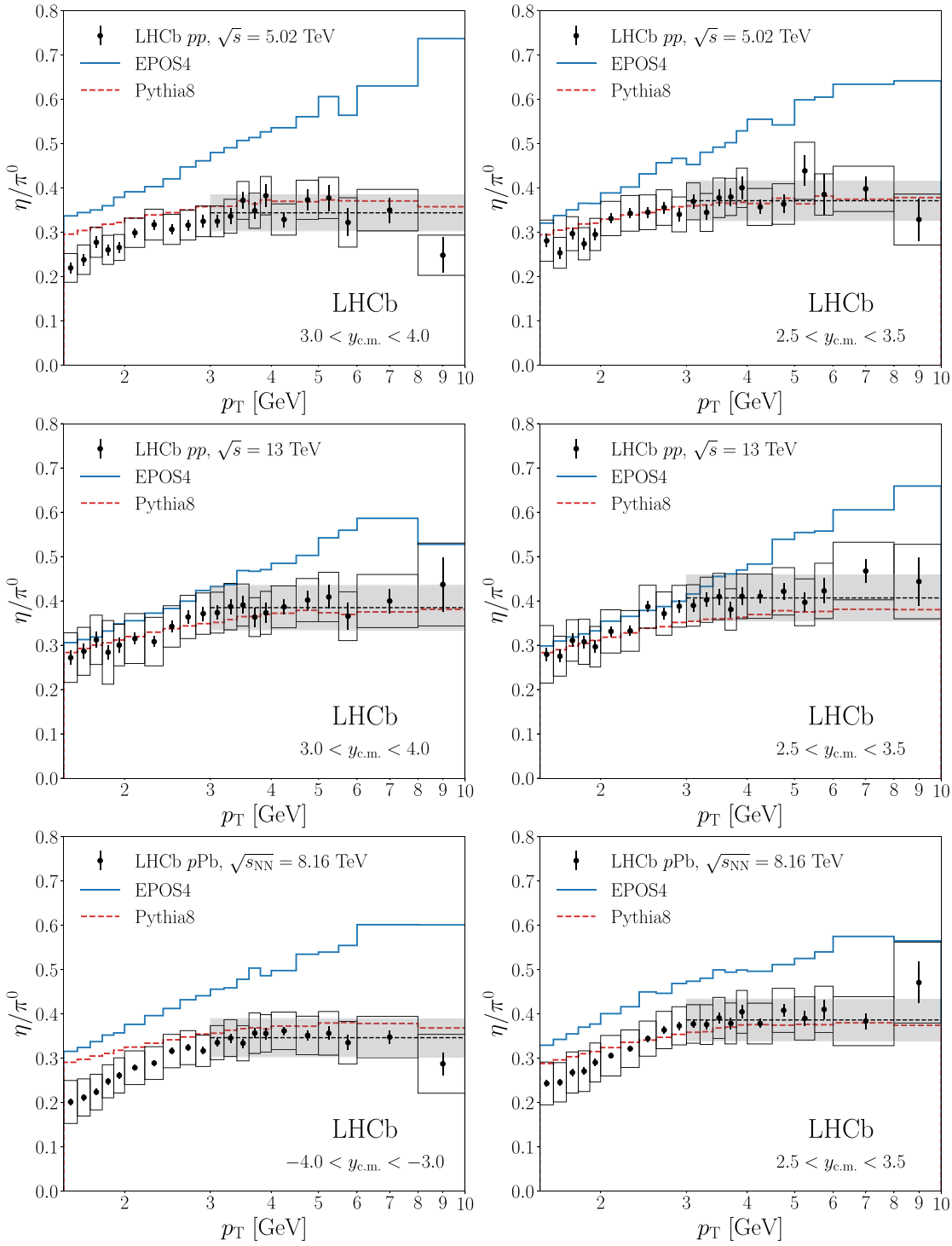

FIG. 8. Measured η/π^0 cross-section ratios in the (left) backward and (right) forward regions. Results are shown for pp collisions at (top) $\sqrt{s} = 5.02$ and (middle) 13 TeV, and (bottom) for pPb collisions at $\sqrt{s_{\rm NN}} = 8.16$ TeV. Results are compared with predictions from EPOS4 and PYTHIA8. The statistical uncertainties are shown by error bars, while systematic uncertainties are shown by boxes. The systematic uncertainties are approximately fully correlated between $p_{\rm T}$ regions. The black dashed line and the gray shaded region show the central value of C^{η/π^0} and its uncertainty, respectively, where C^{η/π^0} is calculated for $p_{\rm T} > 3$ GeV.

the fit while varying the $R^{\eta}_{p\rm Pb}$ by its systematic uncertainties, assuming they are fully correlated in $p_{\rm T}$. The resulting uncertainties are small relative to the $R^{\eta'}_{p\rm Pb}$ uncertainties. The results are compared with predictions from EPOS4 with and without QGP-like effects. The forward results show better agreement with predictions without QGP-like effects, while the backward results are in agreement with both sets of predictions.

The differential cross sections are compared with calculations from PYTHIA8 and EPOS4 in Figs. 6 and 7. The EPOS4 predictions include the effects of hydrodynamic evolution and statistical hadronization for both pp and pPb collisions and use a preliminary tune for pPb collisions. The pPb PYTHIA8 predictions are calculated by scaling pp predictions at $\sqrt{s} = 8.16$ TeV by $A = 208$. The PYTHIA8 predictions provide a good description of the η results at $\sqrt{s} = 5.02$ TeV and at $\sqrt{s} = 13$ TeV in the forward region, but overestimate the η meson yields at $\sqrt{s} = 13$ TeV in the backward region. The PYTHIA8 calculations do not use nPDFs or include other nuclear effects, resulting in disagreement with the pPb data. The EPOS4 predictions consistently overestimate the η cross section in pp collisions but offer a good description of the backward pPb results at low p_{T} and the forward pPb results over the entire p_{T} range. The η' results generally agree with both the EPOS4 and PYTHIA8 predictions, although the measurement uncertainties are large.

The measured η differential cross sections are combined with π^0 differential cross sections from Ref. [19] to calculate η/π^0 cross section ratios. These ratios are presented in Fig. 8 and tabulated in Tables X and XI. The η measurement was performed using only photons reconstructed as ECAL clusters, while the π^0 measurements were performed using combinations of ECAL photons and converted photons. Furthermore, the two measurements use different selection criteria for ECAL photons. As a result, the systematic uncertainties between the two measurements are treated as uncorrelated except for the luminosity uncertainty, which cancels in the cross-section ratio. The measured η/π^0 ratios are compared with predictions from PYTHIA8 and EPOS4. PYTHIA8 generally describes the data well, while EPOS4 generally overestimates the η/π^0 ratio, especially at high p_{T}.

The η/π^0 ratio tends to plateau at p_{T} above a few GeV, and the ratio is often characterized by its plateau height C^{η/π^0}, which is calculated here as the average η/π^0 ratio for $p_{\mathrm{T}} > 3$ GeV. This plateau height is illustrated in Fig. 8 and tabulated in Table XII. Previous studies of the η/π^0 ratio find C^{η/π^0} values of 0.45–0.50, regardless of the species of the colliding nuclei and the center-of-mass energy of the collision [55]. This robustness to changes in experimental conditions illustrates the universality of fragmentation functions in hadron collisions. The values of C^{η/π^0} from this study are lower than the universal average, with C^{η/π^0} decreasing as absolute rapidity increases and as $\sqrt{s_{(\mathrm{NN})}}$ decreases. The ratio of the η meson fragmentation function to that of the π^0 meson differs with the fragmenting parton species, so the variation seen in this measurement can be explained by changes in the flavor of produced partons due to the kinematic dependence of parton distribution functions [56]. Furthermore, the ratio of fragmentation functions varies with z, the momentum fraction of the parton carried by the fragmentation product. The data presented here occupy an extreme kinematic regime and provide access to previously unexplored combinations of z and initial-state parton densities. As a result, these data will provide new constraints in future global analyses of the η meson fragmentation function.

VI. SUMMARY

This article reports the η and η' meson differential cross sections at forward and backward rapidity in pp collisions at $\sqrt{s} = 5.02$ and 13 TeV, as well as in pPb collisions at $\sqrt{s_{\mathrm{NN}}} = 8.16$ TeV collected by the LHCb experiment. This is the first study of η meson production at forward and backward rapidity at the LHC and the first study of η' meson production in high-energy proton-ion collisions. The measured differential cross sections are compared with predictions from PYTHIA8 and EPOS4. Neither event generator successfully describes the measurements for every dataset and rapidity region. This disagreement reflects a lack of previously available light-hadron production data at LHC energies and forward rapidity.

The η meson differential cross sections are used to calculate the η/π^0 cross-section ratio. The measured η/π^0 ratios show evidence of deviation from the universal behavior observed at central rapidity. This deviation indicates that these data are sensitive to the η fragmentation functions in a complementary kinematic regime to previous studies of η production in hadron collisions. The η and η' nuclear modification factors are also reported. The measured nuclear modification factors of the π^0, η, and η' mesons all agree at both forward and backward rapidity for $p_{\mathrm{T}} > 3$ GeV. These data provide limits on the mass dependence of nuclear effects such as radial flow in pPb collisions. Consequently, these data will aid in the interpretation of baryon and strangeness enhancement studies in small-collision systems.

ACKNOWLEDGMENTS

We express our gratitude to our colleagues in the CERN accelerator departments for the excellent performance of the LHC. We thank the technical and administrative staff at the LHCb institutes. We acknowledge support from CERN and from the national agencies: CAPES, CNPq, FAPERJ and FINEP (Brazil); MOST and NSFC (China); CNRS/IN2P3 (France); BMBF, DFG and MPG (Germany); INFN (Italy); NWO (Netherlands); MNiSW and NCN (Poland); MCID/IFA (Romania); MICINN (Spain); SNSF and SER (Switzerland); NASU (Ukraine); STFC (United Kingdom); DOE NP and NSF (USA). We acknowledge the computing resources that are provided by CERN, IN2P3 (France), KIT and DESY (Germany), INFN (Italy), SURF (Netherlands), PIC (Spain), GridPP (United Kingdom), CSCS (Switzerland), IFIN-HH (Romania), CBPF (Brazil), and Polish WLCG (Poland). We are indebted to the communities behind the multiple open-source software packages on which we depend. Individual groups or members have received support from ARC and ARDC (Australia); Key Research Program of Frontier Sciences of CAS, CAS PIFI, CAS CCEPP, Fundamental Research Funds for the Central Universities, and Sci. & Tech. Program of Guangzhou (China); Minciencias (Colombia); EPLANET, Marie Skłodowska-Curie Actions, ERC and NextGenerationEU (European Union); A*MIDEX, ANR, IPhU and Labex P2IO, and Région Auvergne-Rhône-Alpes (France); AvH Foundation (Germany); ICSC (Italy); GVA, XuntaGal, GENCAT, Inditex, InTalent and Prog. Atracción Talento, CM (Spain); SRC (Sweden); the Leverhulme Trust, the Royal Society and UKRI (United Kingdom).

APPENDIX

TABLE III. Measured $d\sigma/dp_T$ of η production in pp collisions at $\sqrt{s} = 13$ TeV. Results and uncertainties are given in mb/GeV. The first uncertainty is statistical and the second is systematic. The statistical uncertainty is uncorrelated between p_T intervals, while the systematic uncertainty is approximately fully correlated.

p_T (GeV)	$2.5 < y_{c.m.} < 3.5$	$3.0 < y_{c.m.} < 4.0$
1.5–1.6	$3.76 \pm 0.19 \pm 0.76$	$3.17 \pm 0.19 \pm 0.68$
1.6–1.7	$2.95 \pm 0.14 \pm 0.42$	$2.66 \pm 0.15 \pm 0.46$
1.7–1.8	$2.56 \pm 0.12 \pm 0.38$	$2.18 \pm 0.12 \pm 0.39$
1.8–1.9	$2.05 \pm 0.09 \pm 0.29$	$1.61 \pm 0.09 \pm 0.34$
1.9–2.0	$1.62 \pm 0.07 \pm 0.22$	$1.40 \pm 0.07 \pm 0.20$
2.0–2.2	$1.30 \pm 0.04 \pm 0.17$	$1.03 \pm 0.04 \pm 0.17$
2.2–2.4	$0.88 \pm 0.03 \pm 0.11$	$0.70 \pm 0.03 \pm 0.11$
2.4–2.6	$0.719 \pm 0.021 \pm 0.083$	$0.531 \pm 0.019 \pm 0.069$
2.6–2.8	$0.508 \pm 0.016 \pm 0.059$	$0.397 \pm 0.015 \pm 0.050$
2.8–3.0	$0.387 \pm 0.012 \pm 0.043$	$0.297 \pm 0.012 \pm 0.034$
3.0–3.2	$0.294 \pm 0.009 \pm 0.032$	$0.221 \pm 0.008 \pm 0.025$
3.2–3.4	$0.230 \pm 0.008 \pm 0.025$	$0.175 \pm 0.007 \pm 0.021$
3.4–3.6	$0.171 \pm 0.006 \pm 0.019$	$0.128 \pm 0.006 \pm 0.014$
3.6–3.8	$0.127 \pm 0.005 \pm 0.013$	$(9.55 \pm 0.51 \pm 0.93) \times 10^{-2}$
3.8–4.0	$0.103 \pm 0.004 \pm 0.010$	$(7.36 \pm 0.38 \pm 0.83) \times 10^{-2}$
4.0–4.5	$(7.04 \pm 0.20 \pm 0.75) \times 10^{-2}$	$(5.09 \pm 0.18 \pm 0.53) \times 10^{-2}$
4.5–5.0	$(4.32 \pm 0.15 \pm 0.43) \times 10^{-2}$	$(3.01 \pm 0.14 \pm 0.32) \times 10^{-2}$
5.0–5.5	$(2.60 \pm 0.11 \pm 0.27) \times 10^{-2}$	$(2.01 \pm 0.11 \pm 0.23) \times 10^{-2}$
5.5–6.0	$(1.63 \pm 0.08 \pm 0.18) \times 10^{-2}$	$(1.05 \pm 0.07 \pm 0.14) \times 10^{-2}$
6.0–8.0	$(6.86 \pm 0.31 \pm 0.74) \times 10^{-3}$	$(4.72 \pm 0.26 \pm 0.65) \times 10^{-3}$
8.0–10.0	$(2.01 \pm 0.21 \pm 0.29) \times 10^{-3}$	$(1.50 \pm 0.17 \pm 0.27) \times 10^{-3}$

TABLE IV. Measured $d\sigma/dp_T$ of η production in pPb collisions at $\sqrt{s_{NN}} = 8.16$ TeV. Results and uncertainties are given in mb/GeV. The first uncertainty is statistical and the second is systematic. The statistical uncertainty is uncorrelated between p_T intervals, while the systematic uncertainty is approximately fully correlated.

p_T (GeV)	$2.5 < y_{c.m.} < 3.5$	$-4.0 < y_{c.m.} < -3.0$
1.5–1.6	$342 \pm 10 \pm 61$	$387 \pm 12 \pm 85$
1.6–1.7	$274 \pm 7 \pm 44$	$320 \pm 9 \pm 59$
1.7–1.8	$237 \pm 6 \pm 38$	$271 \pm 8 \pm 45$
1.8–1.9	$193 \pm 5 \pm 31$	$237 \pm 7 \pm 32$
1.9–2.0	$171 \pm 4 \pm 24$	$201 \pm 5 \pm 28$
2.0–2.2	$130 \pm 2 \pm 18$	$162 \pm 3 \pm 20$
2.2–2.4	$97 \pm 2 \pm 11$	$113 \pm 2 \pm 13$
2.4–2.6	$72.4 \pm 1.2 \pm 7.8$	$87.8 \pm 1.6 \pm 9.1$
2.6–2.8	$54.1 \pm 0.9 \pm 5.5$	$63.0 \pm 1.2 \pm 6.4$
2.8–3.0	$40.4 \pm 0.7 \pm 4.1$	$44.5 \pm 0.9 \pm 4.3$
3.0–3.2	$30.7 \pm 0.6 \pm 3.1$	$34.9 \pm 0.7 \pm 3.5$
3.2–3.4	$23.5 \pm 0.4 \pm 2.4$	$26.5 \pm 0.6 \pm 2.7$
3.4–3.6	$18.2 \pm 0.4 \pm 1.8$	$18.9 \pm 0.4 \pm 1.9$
3.6–3.8	$14.2 \pm 0.3 \pm 1.5$	$15.2 \pm 0.4 \pm 1.6$
3.8–4.0	$11.2 \pm 0.3 \pm 1.2$	$11.9 \pm 0.3 \pm 1.2$
4.0–4.5	$7.39 \pm 0.13 \pm 0.77$	$7.77 \pm 0.15 \pm 0.77$
4.5–5.0	$4.39 \pm 0.09 \pm 0.45$	$4.31 \pm 0.10 \pm 0.41$
5.0–5.5	$2.74 \pm 0.07 \pm 0.27$	$2.61 \pm 0.07 \pm 0.26$
5.5–6.0	$1.66 \pm 0.06 \pm 0.17$	$1.61 \pm 0.05 \pm 0.16$
6.0–8.0	$0.722 \pm 0.021 \pm 0.077$	$0.655 \pm 0.018 \pm 0.060$
8.0–10.0	$0.237 \pm 0.016 \pm 0.039$	$0.159 \pm 0.010 \pm 0.028$

TABLE V. Measured $d\sigma/dp_T$ of η' production in pp collisions at $\sqrt{s} = 5.02$ TeV. Results and uncertainties are given in mb/GeV. The first uncertainty is statistical and the second is systematic. The statistical uncertainty is uncorrelated between p_T bins, while the systematic uncertainty is approximately fully correlated.

p_T (GeV)	$2.5 < y_{c.m.} < 3.5$	$3.0 < y_{c.m.} < 4.0$
3–4	$(2.64 \pm 0.50 \pm 0.84) \times 10^{-2}$	$(2.04 \pm 0.32 \pm 0.74) \times 10^{-2}$
4–5	$(9.0 \pm 1.3 \pm 1.9) \times 10^{-3}$	$(6.7 \pm 0.9 \pm 2.2) \times 10^{-3}$
5–7	$(1.95 \pm 0.10 \pm 0.45) \times 10^{-3}$	$(1.67 \pm 0.24 \pm 0.51) \times 10^{-3}$
7–10	$(3.75 \pm 0.96 \pm 0.85) \times 10^{-4}$	$(2.89 \pm 0.76 \pm 0.74) \times 10^{-4}$

TABLE VI. Measured $d\sigma/dp_T$ of η' production in pp collisions at $\sqrt{s} = 13$ TeV. Results and uncertainties are given in mb/GeV. The first uncertainty is statistical and the second is systematic. The statistical uncertainty is uncorrelated between p_T bins, while the systematic uncertainty is approximately fully correlated.

p_T (GeV)	$2.5 < y_{c.m.} < 3.5$	$3.0 < y_{c.m.} < 4.0$
3–4	$(5.7 \pm 0.9 \pm 1.5) \times 10^{-2}$	$(4.0 \pm 0.6 \pm 1.1) \times 10^{-2}$
4–5	$(2.05 \pm 0.23 \pm 0.58) \times 10^{-2}$	$(1.51 \pm 0.15 \pm 0.53) \times 10^{-2}$
5–7	$(6.5 \pm 0.5 \pm 1.3) \times 10^{-3}$	$(4.33 \pm 0.39 \pm 0.92) \times 10^{-3}$
7–10	$(1.61 \pm 0.16 \pm 0.41) \times 10^{-3}$	$(9.1 \pm 1.2 \pm 2.1) \times 10^{-4}$

TABLE VII. Measured $d\sigma/dp_T$ of η' production in pPb collisions at $\sqrt{s_{NN}} = 8.16$ TeV. Results and uncertainties are given in mb/GeV. The first uncertainty is statistical and the second is systematic. The statistical uncertainty is uncorrelated between p_T bins, while the systematic uncertainty is approximately fully correlated.

p_T (GeV)	$2.5 < y_{c.m.} < 3.5$	$-4.0 < y_{c.m.} < -3.0$
3–4	$5.8 \pm 0.5 \pm 2.1$	$6.0 \pm 1.0 \pm 1.6$
4–5	$1.82 \pm 0.12 \pm 0.56$	$2.14 \pm 0.2 \pm 0.49$
5–7	$0.61 \pm 0.03 \pm 0.15$	$0.68 \pm 0.04 \pm 0.17$
7–10	$0.128 \pm 0.009 \pm 0.027$	$0.111 \pm 0.008 \pm 0.018$

TABLE VIII. Measured η nuclear modification factor $R_{p\mathrm{Pb}}$ as a function of p_T. The first uncertainty is statistical and the second is systematic. The statistical uncertainty is uncorrelated between p_T bins, while the systematic uncertainty is approximately fully correlated.

p_T (GeV)	$2.5 < y_{c.m.} < 3.5$	$-4.0 < y_{c.m.} < -3.0$
1.5–1.6	$0.552 \pm 0.025 \pm 0.033$	$0.807 \pm 0.041 \pm 0.067$
1.6–1.7	$0.589 \pm 0.025 \pm 0.047$	$0.790 \pm 0.038 \pm 0.052$
1.7–1.8	$0.580 \pm 0.024 \pm 0.045$	$0.791 \pm 0.036 \pm 0.046$
1.8–1.9	$0.617 \pm 0.025 \pm 0.044$	$0.939 \pm 0.043 \pm 0.054$
1.9–2.0	$0.667 \pm 0.026 \pm 0.047$	$0.943 \pm 0.040 \pm 0.058$
2.0–2.2	$0.639 \pm 0.017 \pm 0.044$	$1.005 \pm 0.031 \pm 0.049$
2.2–2.4	$0.695 \pm 0.019 \pm 0.043$	$1.015 \pm 0.031 \pm 0.048$
2.4–2.6	$0.691 \pm 0.018 \pm 0.040$	$1.117 \pm 0.033 \pm 0.042$
2.6–2.8	$0.718 \pm 0.020 \pm 0.042$	$1.106 \pm 0.034 \pm 0.043$
2.8–3.0	$0.746 \pm 0.023 \pm 0.042$	$1.056 \pm 0.035 \pm 0.039$
3.0–3.2	$0.725 \pm 0.022 \pm 0.041$	$1.125 \pm 0.038 \pm 0.040$
3.2–3.4	$0.761 \pm 0.025 \pm 0.044$	$1.110 \pm 0.040 \pm 0.048$
3.4–3.6	$0.778 \pm 0.026 \pm 0.044$	$1.028 \pm 0.038 \pm 0.048$
3.6–3.8	$0.771 \pm 0.028 \pm 0.051$	$1.112 \pm 0.046 \pm 0.059$
3.8–4.0	$0.772 \pm 0.031 \pm 0.056$	$1.111 \pm 0.050 \pm 0.051$
4.0–4.5	$0.787 \pm 0.023 \pm 0.049$	$1.143 \pm 0.038 \pm 0.047$
4.5–5.0	$0.777 \pm 0.028 \pm 0.050$	$1.066 \pm 0.042 \pm 0.036$
5.0–5.5	$0.791 \pm 0.034 \pm 0.050$	$0.994 \pm 0.046 \pm 0.047$
5.5–6.0	$0.799 \pm 0.053 \pm 0.064$	$1.210 \pm 0.072 \pm 0.095$
6.0–8.0	$0.830 \pm 0.037 \pm 0.057$	$1.084 \pm 0.053 \pm 0.064$
8.0–10.0	$1.05 \pm 0.11 \pm 0.12$	$1.01 \pm 0.11 \pm 0.15$

TABLE IX. Measured η' nuclear modification factor $R_{p\mathrm{Pb}}$ as a function of p_{T}. The first uncertainty is statistical and the second is systematic. The statistical uncertainty is uncorrelated between p_{T} bins, while the systematic uncertainty is approximately fully correlated.

p_{T} (GeV)	$2.5 < y_{\mathrm{c.m.}} < 3.5$	$-4.0 < y_{\mathrm{c.m.}} < -3.0$
3.0–4.0	$0.71 \pm 0.10 \pm 0.08$	$1.00 \pm 0.19 \pm 0.18$
4.0–5.0	$0.639 \pm 0.073 \pm 0.079$	$1.01 \pm 0.13 \pm 0.18$
5.0–7.0	$0.814 \pm 0.055 \pm 0.093$	$1.21 \pm 0.12 \pm 0.15$
7.0–10.0	$0.78 \pm 0.12 \pm 0.15$	$1.02 \pm 0.17 \pm 0.30$

TABLE X. Measured η/π^0 cross-section ratio for $2.5 < y_{\mathrm{c.m.}} < 3.5$. The first uncertainty is statistical and the second is systematic. The statistical uncertainty is uncorrelated between p_{T} bins, while the systematic uncertainty is approximately fully correlated.

p_{T} (GeV)	5.02 TeV pp	13 TeV pp	8.16 TeV pPb
1.5–1.6	$0.281 \pm 0.014 \pm 0.047$	$0.279 \pm 0.015 \pm 0.060$	$0.246 \pm 0.008 \pm 0.049$
1.6–1.7	$0.253 \pm 0.013 \pm 0.035$	$0.275 \pm 0.014 \pm 0.045$	$0.248 \pm 0.007 \pm 0.045$
1.7–1.8	$0.297 \pm 0.013 \pm 0.038$	$0.311 \pm 0.015 \pm 0.050$	$0.270 \pm 0.008 \pm 0.047$
1.8–1.9	$0.274 \pm 0.013 \pm 0.036$	$0.308 \pm 0.014 \pm 0.047$	$0.273 \pm 0.008 \pm 0.046$
1.9–2.0	$0.295 \pm 0.013 \pm 0.036$	$0.297 \pm 0.014 \pm 0.045$	$0.293 \pm 0.008 \pm 0.044$
2.0–2.2	$0.331 \pm 0.011 \pm 0.039$	$0.331 \pm 0.011 \pm 0.048$	$0.309 \pm 0.006 \pm 0.046$
2.2–2.4	$0.343 \pm 0.011 \pm 0.040$	$0.332 \pm 0.011 \pm 0.046$	$0.325 \pm 0.007 \pm 0.043$
2.4–2.6	$0.345 \pm 0.012 \pm 0.039$	$0.387 \pm 0.012 \pm 0.048$	$0.348 \pm 0.007 \pm 0.040$
2.6–2.8	$0.356 \pm 0.013 \pm 0.040$	$0.371 \pm 0.013 \pm 0.048$	$0.367 \pm 0.008 \pm 0.043$
2.8–3.0	$0.340 \pm 0.015 \pm 0.039$	$0.388 \pm 0.014 \pm 0.048$	$0.377 \pm 0.009 \pm 0.043$
3.0–3.2	$0.370 \pm 0.015 \pm 0.042$	$0.390 \pm 0.014 \pm 0.047$	$0.381 \pm 0.010 \pm 0.044$
3.2–3.4	$0.345 \pm 0.017 \pm 0.043$	$0.402 \pm 0.016 \pm 0.051$	$0.380 \pm 0.010 \pm 0.045$
3.4–3.6	$0.378 \pm 0.018 \pm 0.045$	$0.410 \pm 0.017 \pm 0.053$	$0.395 \pm 0.012 \pm 0.047$
3.6–3.8	$0.380 \pm 0.020 \pm 0.042$	$0.381 \pm 0.018 \pm 0.046$	$0.382 \pm 0.013 \pm 0.047$
3.8–4.0	$0.400 \pm 0.025 \pm 0.045$	$0.410 \pm 0.020 \pm 0.050$	$0.409 \pm 0.015 \pm 0.049$
4.0–4.5	$0.357 \pm 0.016 \pm 0.042$	$0.410 \pm 0.015 \pm 0.050$	$0.382 \pm 0.011 \pm 0.046$
4.5–5.0	$0.364 \pm 0.021 \pm 0.046$	$0.422 \pm 0.018 \pm 0.053$	$0.412 \pm 0.014 \pm 0.050$
5.0–5.5	$0.439 \pm 0.034 \pm 0.064$	$0.397 \pm 0.022 \pm 0.053$	$0.394 \pm 0.017 \pm 0.049$
5.5–6.0	$0.385 \pm 0.045 \pm 0.047$	$0.423 \pm 0.028 \pm 0.062$	$0.414 \pm 0.022 \pm 0.053$
6.0–8.0	$0.398 \pm 0.027 \pm 0.051$	$0.467 \pm 0.026 \pm 0.064$	$0.388 \pm 0.018 \pm 0.056$
8.0–10.0	$0.329 \pm 0.047 \pm 0.057$	$0.444 \pm 0.054 \pm 0.079$	$0.475 \pm 0.047 \pm 0.092$

TABLE XI. Measured η/π^0 cross-section ratio for $-4.0 < y_{\mathrm{c.m.}} < -3.0$. The first uncertainty is statistical and the second is systematic. The statistical uncertainty is uncorrelated between p_{T} bins, while the systematic uncertainty is approximately fully correlated.

p_{T} (GeV)	5.02 TeV pp	13 TeV pp	8.16 TeV pPb
1.5–1.6	$0.219 \pm 0.012 \pm 0.032$	$0.272 \pm 0.016 \pm 0.061$	$0.197 \pm 0.007 \pm 0.047$
1.6–1.7	$0.238 \pm 0.013 \pm 0.033$	$0.286 \pm 0.017 \pm 0.053$	$0.209 \pm 0.007 \pm 0.042$
1.7–1.8	$0.277 \pm 0.013 \pm 0.034$	$0.312 \pm 0.018 \pm 0.059$	$0.224 \pm 0.007 \pm 0.040$
1.8–1.9	$0.260 \pm 0.012 \pm 0.033$	$0.284 \pm 0.016 \pm 0.062$	$0.248 \pm 0.007 \pm 0.037$
1.9–2.0	$0.266 \pm 0.012 \pm 0.029$	$0.300 \pm 0.016 \pm 0.047$	$0.256 \pm 0.007 \pm 0.039$
2.0–2.2	$0.299 \pm 0.010 \pm 0.033$	$0.315 \pm 0.013 \pm 0.055$	$0.276 \pm 0.006 \pm 0.038$
2.2–2.4	$0.317 \pm 0.011 \pm 0.035$	$0.308 \pm 0.012 \pm 0.051$	$0.286 \pm 0.006 \pm 0.036$
2.4–2.6	$0.306 \pm 0.011 \pm 0.034$	$0.342 \pm 0.013 \pm 0.048$	$0.314 \pm 0.007 \pm 0.037$
2.6–2.8	$0.316 \pm 0.012 \pm 0.034$	$0.364 \pm 0.015 \pm 0.049$	$0.323 \pm 0.007 \pm 0.038$
2.8–3.0	$0.325 \pm 0.014 \pm 0.035$	$0.371 \pm 0.016 \pm 0.047$	$0.320 \pm 0.008 \pm 0.036$
3.0–3.2	$0.325 \pm 0.014 \pm 0.035$	$0.373 \pm 0.016 \pm 0.047$	$0.336 \pm 0.009 \pm 0.038$
3.2–3.4	$0.336 \pm 0.017 \pm 0.038$	$0.387 \pm 0.017 \pm 0.053$	$0.345 \pm 0.009 \pm 0.041$
3.4–3.6	$0.372 \pm 0.019 \pm 0.043$	$0.391 \pm 0.020 \pm 0.048$	$0.337 \pm 0.010 \pm 0.040$
3.6–3.8	$0.348 \pm 0.019 \pm 0.040$	$0.363 \pm 0.022 \pm 0.042$	$0.357 \pm 0.011 \pm 0.046$
3.8–4.0	$0.382 \pm 0.026 \pm 0.043$	$0.373 \pm 0.022 \pm 0.048$	$0.359 \pm 0.012 \pm 0.043$
4.0–4.5	$0.329 \pm 0.017 \pm 0.035$	$0.387 \pm 0.017 \pm 0.048$	$0.364 \pm 0.009 \pm 0.042$
4.5–5.0	$0.373 \pm 0.023 \pm 0.044$	$0.402 \pm 0.022 \pm 0.050$	$0.352 \pm 0.011 \pm 0.044$
5.0–5.5	$0.377 \pm 0.029 \pm 0.047$	$0.409 \pm 0.027 \pm 0.056$	$0.357 \pm 0.014 \pm 0.050$
5.5–6.0	$0.322 \pm 0.032 \pm 0.056$	$0.365 \pm 0.030 \pm 0.054$	$0.335 \pm 0.017 \pm 0.048$
6.0–8.0	$0.350 \pm 0.028 \pm 0.047$	$0.400 \pm 0.027 \pm 0.063$	$0.346 \pm 0.014 \pm 0.047$
8.0–10.0	$0.248 \pm 0.040 \pm 0.045$	$0.437 \pm 0.061 \pm 0.093$	$0.281 \pm 0.025 \pm 0.065$

TABLE XII. Measured C^{η/π^0} for each dataset and rapidity region. The first uncertainty is statistical and the second is systematic. The systematic uncertainties are approximately 90% positively correlated between datasets.

	$-4.0 < y_{\text{c.m.}} < -3.0$	$2.5 < y_{\text{c.m.}} < 3.5$
5.02 TeV pp	$0.344 \pm 0.006 \pm 0.040$	$0.371 \pm 0.006 \pm 0.045$
13 TeV pp	$0.385 \pm 0.006 \pm 0.050$	$0.407 \pm 0.006 \pm 0.052$
8.16 TeV pPb	$0.346 \pm 0.004 \pm 0.043$	$0.386 \pm 0.004 \pm 0.047$

[1] K. J. Eskola, P. Paakkinen, H. Paukkunen, and C. A. Salgado, Epps16: Nuclear parton distributions with LHC data, Eur. Phys. J. C **77**, 163 (2017).

[2] D. de Florian, R. Sassot, P. Zurita, and M. Stratmann, Global analysis of nuclear parton distributions, Phys. Rev. D **85**, 074028 (2012).

[3] S. S. Adler *et al.* (PHENIX Collaboration), Centrality dependence of π^0 and η production at large transverse momentum in $\sqrt{s_{\text{NN}}} = 200\text{GeV}d+$ Au collisions, Phys. Rev. Lett. **98**, 172302 (2007).

[4] J. Adams *et al.* (STAR Collaboration), Identified hadron spectra at large transverse momentum in $p + p$ and $d+$ Au collisions at $\sqrt{s_{\text{NN}}} = 200$ GeV, Phys. Lett. B **637**, 161 (2006).

[5] B. I. Abelev *et al.* (STAR Collaboration), Inclusive π^0, η, and direct photon production at high transverse momentum in $p + p$ and $d+$ Au collisions at $\sqrt{s_{NN}} = 200$ GeV, Phys. Rev. C **81**, 064904 (2010).

[6] J. C. Collins, D. E. Soper, and G. F. Sterman, Factorization of hard processes in QCD, Adv. Ser. Direct. High Energy Phys. **5**, 1 (1989).

[7] I. Arsene *et al.* (BRAHMS Collaboration), Quark gluon plasma and color glass condensate at RHIC? The perspective from the BRAHMS experiment, Nucl. Phys. A **757**, 1 (2005).

[8] B. B. Back *et al.* (PHOBOS Collaboration), The PHOBOS perspective on discoveries at RHIC, Nucl. Phys. A **757**, 28 (2005).

[9] J. Adams *et al.* (STAR Collaboration), Experimental and theoretical challenges in the search for the quark gluon plasma: The STAR Collaboration's critical assessment of the evidence from RHIC collisions, Nucl. Phys. A **757**, 102 (2005).

[10] K. Adcox *et al.* (PHENIX Collaboration), Formation of dense partonic matter in relativistic nucleus-nucleus collisions at RHIC: Experimental evaluation by the PHENIX collaboration, Nucl. Phys. A **757**, 184 (2005).

[11] V. Khachatryan *et al.* (CMS Collaboration), Observation of long-range near-side angular correlations in proton-proton collisions at the LHC, J. High Energy Phys. 09 (2010) 091.

[12] B. Abelev *et al.* (ALICE Collaboration), Long-range angular correlations on the near and away side in p-Pb collisions at $\sqrt{s_{NN}} = 5.02$ TeV, Phys. Lett. B **719**, 29 (2013).

[13] G. Aad *et al.* (ATLAS Collaboration), Observation of associated near-side and away-side long-range correlations in $\sqrt{s_{NN}} =$ 5.02 TeV proton-lead collisions with the ATLAS detector, Phys. Rev. Lett. **110**, 182302 (2013).

[14] S. Chatrchyan *et al.* (CMS Collaboration), Observation of long-range near-side angular correlations in proton-lead collisions at the LHC, Phys. Lett. B **718**, 795 (2013).

[15] R. Aaij *et al.* (LHCb Collaboration), Measurements of long-range near-side angular correlations in $\sqrt{s_{\text{NN}}} = 5$ TeV proton-lead collisions in the forward region, Phys. Lett. B **762**, 473 (2016).

[16] A. Adare *et al.* (PHENIX Collaboration), Quadrupole anisotropy in dihadron azimuthal correlations in central $d+$ Au collisions at $\sqrt{s_{NN}} = 200$ GeV, Phys. Rev. Lett. **111**, 212301 (2013).

[17] C. Aidala *et al.* (PHENIX Collaboration), Creation of quark–gluon plasma droplets with three distinct geometries, Nat. Phys. **15**, 214 (2019).

[18] R. Aaij *et al.* (LHCb Collaboration), Measurement of the nuclear modification factor and prompt charged particle production in pPb and pp collisions at $\sqrt{s_{\text{NN}}} = 5$ TeV, Phys. Rev. Lett. **128**, 142004 (2022).

[19] R. Aaij *et al.* (LHCb Collaboration), Nuclear modification of π^0 production in pPb collisions at $\sqrt{s_{\text{NN}}} = 8.16$ TeV, Phys. Rev. Lett. **131**, 042302 (2023).

[20] T. Pierog, Iu. Karpenko, J. M. Katzy, E. Yatsenko, and K. Werner, EPOS LHC: Test of collective hadronization with data measured at the CERN Large Hadron Collider, Phys. Rev. C **92**, 034906 (2015).

[21] A. M. Sickles, Possible evidence for radial flow of heavy mesons in d + Au collisions, Phys. Lett. B **731**, 51 (2014).

[22] A. Ayala, E. Cuautle, J. Magnin, and L. M. Montano, Proton and pion transverse spectra at RHIC from radial flow and finite size effects, Phys. Rev. C **74**, 064903 (2006).

[23] S. Acharya *et al.* (ALICE Collaboration), Multiplicity dependence of π, k, and p production in pp collisions at $\sqrt{s} =$ 13 TeV, Eur. Phys. J. C **80**, 693 (2020).

[24] S. Acharya *et al.* (ALICE Collaboration), Multiplicity dependence of light-flavor hadron production in pp collisions at $\sqrt{s} =$ 7 TeV, Phys. Rev. C **99**, 024906 (2019).

[25] A. Adare *et al.* (PHENIX Collaboration), Measurement of neutral mesons in $p + p$ collisions at $\sqrt{s} = 200$ GeV and scaling properties of hadron production, Phys. Rev. D **83**, 052004 (2011).

[26] A. Adare *et al.* (PHENIX Collaboration), Cross section and double helicity asymmetry for η mesons and their comparison to neutral pion production in $p + p$ collisions at $\sqrt{s} = 200$ GeV, Phys. Rev. D **83**, 032001 (2011).

[27] B. Abelev *et al.* (ALICE Collaboration), Neutral pion and η meson production in proton-proton collisions at $\sqrt{s} = 0.9$ TeV and $\sqrt{s} = 7$ TeV, Phys. Lett. B **717**, 162 (2012).

[28] S. Acharya *et al.* (ALICE Collaboration), π^0 and η meson production in proton-proton collisions at $\sqrt{s} = 8$ TeV, Eur. Phys. J. C **78**, 263 (2018).

[29] S. Acharya *et al.* (ALICE Collaboration), Neutral pion and η meson production in p-Pb collisions at $\sqrt{s_{\text{NN}}} = 5.02$ TeV, Eur. Phys. J. C **78**, 624 (2018).

[30] S. Acharya *et al.* (ALICE Collaboration), Nuclear modification factor of light neutral-meson spectra up to high transverse momentum in p–Pb collisions at $\sqrt{s_{\rm NN}} = 8.16$ TeV, Phys. Lett. B **827**, 136943 (2022).

[31] L. Adamczyk *et al.* (STAR Collaboration), Transverse single-spin asymmetry and cross-section for π^0 and η mesons at large Feynman-x in polarized $p + p$ collisions at $\sqrt{s} = 200$ GeV, Phys. Rev. D **86**, 051101 (2012).

[32] A. Adare *et al.* (PHENIX Collaboration), Cross section and transverse single-spin asymmetry of η mesons in $p^{\uparrow} + p$ collisions at $\sqrt{s} = 200$ GeV at forward rapidity, Phys. Rev. D **90**, 072008 (2014).

[33] A. A. Alves Jr., *et al.* (LHCb Collaboration), The LHCb detector at the LHC, JINST **3**, S08005 (2008).

[34] R. Aaij *et al.* (LHCb Collaboration), LHCb detector performance, Int. J. Mod. Phys. A **30**, 1530022 (2015).

[35] C. Abellan Beteta *et al.*, Calibration and performance of the LHCb calorimeters in Run 1 and 2 at the LHC, arXiv:2008.11556.

[36] T. Sjöstrand, S. Mrenna, and P. Skands, A brief introduction to PYTHIA 8.1, Comput. Phys. Commun. **178**, 852 (2008).

[37] D. J. Lange, The EvtGen particle decay simulation package, Nucl. Instrum. Methods Phys. Res., Sect. A **462**, 152 (2001).

[38] N. Davidson, T. Przedzinski, and Z. Was, PHOTOS interface in C++: Technical and physics documentation, Comput. Phys. Commun. **199**, 86 (2016).

[39] J. Allison *et al.* (Geant4 Collaboration), Geant4 developments and applications, IEEE Trans. Nucl. Sci. **53**, 270 (2006).

[40] S. Agostinelli *et al.* (Geant4 Collaboration), Geant4: A simulation toolkit, Nucl. Instrum. Methods Phys. Res., Sect. A **506**, 250 (2003).

[41] M. Clemencic *et al.*, The LHCb simulation application, Gauss: Design, evolution and experience, J. Phys.: Conf. Ser. **331**, 032023 (2011).

[42] R. Aaij *et al.* (LHCb Collaboration), Measurement of B^+, B^0 and Λ_b^0 production in p Pb collisions at $\sqrt{s_{\rm NN}} = 8.16$ TeV, Phys. Rev. D **99**, 052011 (2019).

[43] R. Aaij *et al.* (LHCb Collaboration), Precision luminosity measurements at LHCb, J. Instrum. **9**, P09007 (2014).

[44] Particle P. D. Group, R. L. Workman *et al.*, Review of particle physics, Prog. Theor. Exp. Phys. **2022**, 083C01 (2022).

[45] H. Dembinski *et al.*, *scikit-hep/iminuit*, 10.5281/zenodo.3949207.

[46] H. Dembinski and A. Abdelmotteleb, A new maximum-likelihood method for template fits, Eur. Phys. J. C **82**, 1043 (2022).

[47] T. Skwarnicki, Ph.D. thesis, Institute of Nuclear Physics, Krakow, 1986 (unpublished).

[48] A. Adare *et al.* (PHENIX Collaboration), Detailed measurement of the e^+e^- pair continuum in $p + p$ and Au + Au collisions at $\sqrt{s_{NN}} = 200$ GeV and implications for direct photon production, Phys. Rev. C **81**, 034911 (2010).

[49] R. Aaij *et al.* (LHCb Collaboration), Measurement of the electron reconstruction efficiency at LHCb, J. Instrum. **14**, P11023 (2019).

[50] V. Khachatryan *et al.* (CMS Collaboration), Nuclear effects on the transverse momentum spectra of charged particles in pPb collisions at $\sqrt{s_{\rm NN}} = 5.02$ TeV, Eur. Phys. J. C **75**, 237 (2015).

[51] N. Armesto, Nuclear shadowing, J. Phys. G **32**, R367 (2006).

[52] K. J. Eskola, P. Paakkinen, H. Paukkunen, and C. A. Salgado, EPPS21: A global QCD analysis of nuclear PDFs, Eur. Phys. J. C **82**, 413 (2022).

[53] R. Abdul Khalek *et al.*, nNNPDF3.0: Evidence for a modified partonic structure in heavy nuclei, Eur. Phys. J. C **82**, 507 (2022).

[54] C. E. Rasmussen and C. K. I. Williams, *Gaussian Processes for Machine Learning* (The MIT Press, Cambridge, Massachusetts, 2005).

[55] Y. Ren and A. Drees, Study of the η to π^0 ratio in heavy-ion collisions, Phys. Rev. C **104**, 054902 (2021).

[56] C. A. Aidala, F. Ellinghaus, R. Sassot, J. P. Seele, and M. Stratmann, Global analysis of fragmentation functions for eta mesons, Phys. Rev. D **83**, 034002 (2011).

R. Aaij[35] A. S. W. Abdelmotteleb[54] C. Abellan Beteta,[48] F. Abudinén[54] T. Ackernley[58] B. Adeva[44] M. Adinolfi[52] P. Adlarson[78] C. Agapopoulou[46] C. A. Aidala[79] Z. Ajaltouni,[11] S. Akar[63] K. Akiba[35] P. Albicocco[25] J. Albrecht[17] F. Alessio[46] M. Alexander[57] A. Alfonso Albero[43] Z. Aliouche[60] P. Alvarez Cartelle[53] R. Amalric[15] S. Amato[3] J. L. Amey[52] Y. Amhis[13,46] L. An[6] L. Anderlini[24] M. Andersson[48] A. Andreianov[41] P. Andreola[48] M. Andreotti[23] D. Andreou[66] A. A. Anelli[28,a] D. Ao[7] F. Archilli[34,b] M. Argenton[23] S. Arguedas Cuendis[9] A. Artamonov[41] M. Artuso[66] E. Aslanides[12] M. Atzeni[62] B. Audurier[14] D. Bacher[61] I. Bachiller Perea[10] S. Bachmann[19] M. Bachmayer[47] J. J. Back[54] A. Bailly-reyre,[15] P. Baladron Rodriguez[44] V. Balagura[14] W. Baldini[23] J. Baptista de Souza Leite[2] M. Barbetti[24,c] I. R. Barbosa[67] R. J. Barlow[60] S. Barsuk[13] W. Barter[56] M. Bartolini[53] F. Baryshnikov[41] J. M. Basels[16] G. Bassi[32,d] B. Batsukh[5] A. Battig[17] A. Bay[47] A. Beck[54] M. Becker[17] F. Bedeschi[32] I. B. Bediaga[2] A. Beiter,[66] S. Belin[44] V. Bellee[48] K. Belous[41] I. Belov[26] I. Belyaev[41] G. Benane[12] G. Bencivenni[25] E. Ben-Haim[15] A. Berezhnoy[41] R. Bernet[48] S. Bernet Andres[42] H. C. Bernstein,[66] C. Bertella[60] A. Bertolin[30] C. Betancourt[48] F. Betti[56] J. Bex[53] Ia. Bezshyiko[48] J. Bhom[38] M. S. Bieker[17] N. V. Biesuz[23] P. Billoir[15] A. Biolchini[35] M. Birch[59] F. C. R. Bishop[10] A. Bitadze[60] A. Bizzeti, M. P. Blago[53] T. Blake[54] F. Blanc[47] J. E. Blank[17] S. Blusk[66] D. Bobulska[57] V. Bocharnikov[41] J. A. Boelhauve[17] O. Boente Garcia[14] T. Boettcher[63] A. Bohare[56] A. Boldyrev[41] C. S. Bolognani[76] R. Bolzonella[23,e] N. Bondar[41] F. Borgato[30,46] S. Borghi[60] M. Borsato[28,a] J. T. Borsuk[38] S. A. Bouchiba[47] T. J. V. Bowcock[58] A. Boyer[46] C. Bozzi[23] M. J. Bradley,[59] S. Braun[64] A. Brea Rodriguez[44] N. Breer[17] J. Brodzicka[38] A. Brossa Gonzalo[44] J. Brown[58] D. Brundu[29] A. Buonaura[48] L. Buonincontri[30] A. T. Burke[60] C. Burr[46] A. Bursche,[69] A. Butkevich[41]

J. S. Butter,[53] J. Buytaert,[46] W. Byczynski,[46] S. Cadeddu,[29] H. Cai,[71] R. Calabrese,[23,e] L. Calefice,[17] S. Cali,[25] M. Calvi,[28,a] M. Calvo Gomez,[42] J. Cambon Bouzas,[44] P. Campana,[25] D. H. Campora Perez,[76] A. F. Campoverde Quezada,[7] S. Capelli,[28,a] L. Capriotti,[23] R. Caravaca-Mora,[9] A. Carbone,[22,f] L. Carcedo Salgado,[44] R. Cardinale,[26,g] A. Cardini,[29] P. Carniti,[28,a] L. Carus,[19] A. Casais Vidal,[62] R. Caspary,[19] G. Casse,[58] J. Castro Godinez,[9] M. Cattaneo,[46] G. Cavallero,[23] V. Cavallini,[23,e] S. Celani,[47] J. Cerasoli,[12] D. Cervenkov,[61] S. Cesare,[27,h] A. J. Chadwick,[58] I. Chahrour,[79] M. Charles,[15] Ph. Charpentier,[46] C. A. Chavez Barajas,[58] M. Chefdeville,[10] C. Chen,[12] S. Chen,[5] A. Chernov,[38] S. Chernyshenko,[50] V. Chobanova,[44,i] S. Cholak,[47] M. Chrzaszcz,[38] A. Chubykin,[41] V. Chulikov,[41] P. Ciambrone,[25] M. F. Cicala,[54] X. Cid Vidal,[44] G. Ciezarek,[46] P. Cifra,[46] P. E. L. Clarke,[56] M. Clemencic,[46] H. V. Cliff,[53] J. Closier,[46] J. L. Cobbledick,[60] C. Cocha Toapaxi,[19] V. Coco,[46] J. Cogan,[12] E. Cogneras,[11] L. Cojocariu,[40] P. Collins,[46] T. Colombo,[46] A. Comerma-Montells,[43] L. Congedo,[21] A. Contu,[29] N. Cooke,[57] I. Corredoira,[44] A. Correia,[15] G. Corti,[46] J. J. Cottee Meldrum,[52] B. Couturier,[46] D. C. Craik,[48] M. Cruz Torres,[2,j] R. Currie,[56] C. L. Da Silva,[65] S. Dadabaev,[41] L. Dai,[68] X. Dai,[6] E. Dall'Occo,[17] J. Dalseno,[44] C. D'Ambrosio,[46] J. Daniel,[11] A. Danilina,[41] P. d'Argent,[21] A. Davidson,[54] J. E. Davies,[60] A. Davis,[60] O. De Aguiar Francisco,[60] C. De Angelis,[29,k] J. de Boer,[35] K. De Bruyn,[75] S. De Capua,[60] M. De Cian,[19,46] U. De Freitas Carneiro Da Graca,[2,l] E. De Lucia,[25] J. M. De Miranda,[2] L. De Paula,[3] M. De Serio,[21,m] D. De Simone,[48] P. De Simone,[25] F. De Vellis,[17] J. A. de Vries,[76] F. Debernardis,[21,m] D. Decamp,[10] V. Dedu,[12] L. Del Buono,[15] B. Delaney,[62] H.-P. Dembinski,[17] J. Deng,[8] V. Denysenko,[48] O. Deschamps,[11] F. Dettori,[29,k] B. Dey,[74] P. Di Nezza,[25] I. Diachkov,[41] S. Didenko,[41] S. Ding,[66] V. Dobishuk,[50] A. D. Docheva,[57] A. Dolmatov,[41] C. Dong,[4] A. M. Donohoe,[20] F. Dordei,[29] A. C. dos Reis,[2] L. Douglas,[57] A. G. Downes,[10] W. Duan,[69] P. Duda,[77] M. W. Dudek,[38] L. Dufour,[46] V. Duk,[31] P. Durante,[46] M. M. Duras,[77] J. M. Durham,[65] A. Dziurda,[38] A. Dzyuba,[41] S. Easo,[55,46] E. Eckstein,[73] U. Egede,[1] A. Egorychev,[41] V. Egorychev,[41] C. Eirea Orro,[44] S. Eisenhardt,[56] E. Ejopu,[60] S. Ek-In,[47] L. Eklund,[78] M. Elashri,[63] J. Ellbracht,[17] S. Ely,[59] A. Ene,[40] E. Epple,[63] S. Escher,[16] J. Eschle,[48] S. Esen,[48] T. Evans,[60] F. Fabiano,[29,46,k] L. N. Falcao,[2] Y. Fan,[7] B. Fang,[71,13] L. Fantini,[31,n] M. Faria,[47] K. Farmer,[56] D. Fazzini,[28,a] L. Felkowski,[77] M. Feng,[5,7] M. Feo,[46] M. Fernandez Gomez,[44] A. D. Fernez,[64] F. Ferrari,[22] F. Ferreira Rodrigues,[3] S. Ferreres Sole,[35] M. Ferrillo,[48] M. Ferro-Luzzi,[46] S. Filippov,[41] R. A. Fini,[21] M. Fiorini,[23,e] M. Firlej,[37] K. M. Fischer,[61] D. S. Fitzgerald,[79] C. Fitzpatrick,[60] T. Fiutowski,[37] F. Fleuret,[14] M. Fontana,[22] F. Fontanelli,[26,g] L. F. Foreman,[60] R. Forty,[46] D. Foulds-Holt,[53] M. Franco Sevilla,[64] M. Frank,[46] E. Franzoso,[23,e] G. Frau,[19] C. Frei,[46] D. A. Friday,[60] L. Frontini,[27,h] J. Fu,[7] Q. Fuehring,[17] Y. Fujii,[1] T. Fulghesu,[15] E. Gabriel,[35] G. Galati,[21,m] M. D. Galati,[35] A. Gallas Torreira,[44] D. Galli,[22,f] S. Gambetta,[56,46] M. Gandelman,[3] P. Gandini,[27] H. Gao,[7] R. Gao,[61] Y. Gao,[8] Y. Gao,[6] Y. Gao,[8] M. Garau,[29,k] L. M. Garcia Martin,[47] P. Garcia Moreno,[43] J. García Pardiñas,[46] B. Garcia Plana,[44] K. G. Garg,[8] L. Garrido,[43] C. Gaspar,[46] R. E. Geertsema,[35] L. L. Gerken,[17] E. Gersabeck,[60] M. Gersabeck,[60] T. Gershon,[54] Z. Ghorbanimoghaddam,[52] L. Giambastiani,[30] F. I. Giasemis,[15,o] V. Gibson,[53] H. K. Giemza,[39] A. L. Gilman,[61] M. Giovannetti,[25] A. Gioventù,[43] P. Gironella Gironell,[43] C. Giugliano,[23,e] M. A. Giza,[38] E. L. Gkougkousis,[59] F. C. Glaser,[13,19] V. V. Gligorov,[15] C. Göbel,[67] E. Golobardes,[42] D. Golubkov,[41] A. Golutvin,[59,41,46] A. Gomes,[2,p,q] S. Gomez Fernandez,[43] F. Goncalves Abrantes,[61] M. Goncerz,[38] G. Gong,[4] J. A. Gooding,[17] I. V. Gorelov,[41] C. Gotti,[28] J. P. Grabowski,[73] L. A. Granado Cardoso,[46] E. Graugés,[43] E. Graverini,[47] L. Grazette,[54] G. Graziani, A. T. Grecu,[40] L. M. Greeven,[35] N. A. Grieser,[63] L. Grillo,[57] S. Gromov,[41] C. Gu,[14] M. Guarise,[23] M. Guittiere,[13] V. Guliaeva,[41] P. A. Günther,[19] A.-K. Guseinov,[41] E. Gushchin,[41] Y. Guz,[6,41,46] T. Gys,[46] T. Hadavizadeh,[1] C. Hadjivasiliou,[64] G. Haefeli,[47] C. Haen,[46] J. Haimberger,[46] M. Hajheidari,[46] T. Halewood-leagas,[58] M. M. Halvorsen,[46] P. M. Hamilton,[64] J. Hammerich,[58] Q. Han,[8] X. Han,[19] S. Hansmann-Menzemer,[19] L. Hao,[7] N. Harnew,[61] T. Harrison,[58] M. Hartmann,[13] C. Hasse,[46] J. He,[7,r] K. Heijhoff,[35] F. Hemmer,[46] C. Henderson,[63] R. D. L. Henderson,[1,54] A. M. Hennequin,[46] K. Hennessy,[58] L. Henry,[47] J. Herd,[59] J. Heuel,[16] A. Hicheur,[3] D. Hill,[47] S. E. Hollitt,[17] J. Horswill,[60] R. Hou,[8] Y. Hou,[10] N. Howarth,[58] J. Hu,[19] J. Hu,[69] W. Hu,[6] X. Hu,[4] W. Huang,[7] W. Hulsbergen,[35] R. J. Hunter,[54] M. Hushchyn,[41] D. Hutchcroft,[58] M. Idzik,[37] D. Ilin,[41] P. Ilten,[63] A. Inglessi,[41] A. Iniukhin,[41] A. Ishteev,[41] K. Ivshin,[41] R. Jacobsson,[46] H. Jage,[16] S. J. Jaimes Elles,[45,72] S. Jakobsen,[46] E. Jans,[35] B. K. Jashal,[45] A. Jawahery,[64] V. Jevtic,[17] E. Jiang,[64] X. Jiang,[5,7] Y. Jiang,[7] Y. J. Jiang,[6] M. John,[61] D. Johnson,[51] C. R. Jones,[53] T. P. Jones,[54] S. Joshi,[39] B. Jost,[46] N. Jurik,[46] I. Juszczak,[38] D. Kaminaris,[47] S. Kandybei,[49] Y. Kang,[4] M. Karacson,[46] D. Karpenkov,[41] M. Karpov,[41] A. M. Kauniskangas,[47] J. W. Kautz,[63] F. Keizer,[46] D. M. Keller,[66] M. Kenzie,[53] T. Ketel,[35] A. Khanal,[63] B. Khanji,[66] A. Kharisova,[41] S. Kholodenko,[32] G. Khreich,[13] T. Kirn,[16] V. S. Kirsebom,[47] O. Kitouni,[62] S. Klaver,[36] N. Kleijne,[32,d] K. Klimaszewski,[39] M. R. Kmiec,[39] S. Koliiev,[50] L. Kolk,[17] A. Konoplyannikov,[41] P. Kopciewicz,[37,46] P. Koppenburg,[35] M. Korolev,[41] I. Kostiuk,[35] O. Kot,[50] S. Kotriakhova, A. Kozachuk,[41] P. Kravchenko,[41] L. Kravchuk,[41] M. Kreps,[54] S. Kretzschmar,[16] P. Krokovny,[41] W. Krupa,[66] W. Krzemien,[39] J. Kubat,[19] S. Kubis,[77] W. Kucewicz,[38] M. Kucharczyk,[38] V. Kudryavtsev,[41] E. Kulikova,[41] A. Kupsc,[78] B. K. Kutsenko,[12] D. Lacarrere,[46] A. Lai,[29] A. Lampis,[29] D. Lancierini,[48] C. Landesa Gomez,[44] J. J. Lane,[1] R. Lane,[52] C. Langenbruch,[19] J. Langer,[17] O. Lantwin,[41] T. Latham,[54]

F. Lazzari,[32,s] C. Lazzeroni,[51] R. Le Gac,[12] S. H. Lee,[79] R. Lefèvre,[11] A. Leflat,[41] S. Legotin,[41] M. Lehuraux,[54] O. Leroy,[12] T. Lesiak,[38] B. Leverington,[19] A. Li,[4] H. Li,[69] K. Li,[8] L. Li,[60] P. Li,[46] P.-R. Li,[70] S. Li,[8] T. Li,[5] T. Li,[69] Y. Li,[8] Y. Li,[5] Z. Li,[66] Z. Lian,[4] X. Liang,[66] C. Lin,[7] T. Lin,[55] R. Lindner,[46] V. Lisovskyi,[47] R. Litvinov,[29,k] G. Liu,[69] H. Liu,[7] K. Liu,[70] Q. Liu,[7] S. Liu,[5,7] Y. Liu,[56] Y. Liu,[70] Y. L. Liu,[59] A. Lobo Salvia,[43] A. Loi,[29] J. Lomba Castro,[44] T. Long,[53] J. H. Lopes,[3] A. Lopez Huertas,[43] S. López Soliño,[44] G. H. Lovell,[53] C. Lucarelli,[24,c] D. Lucchesi,[30,t] S. Luchuk,[41] M. Lucio Martinez,[76] V. Lukashenko,[35,50] Y. Luo,[4] A. Lupato,[30] E. Luppi,[23,e] K. Lynch,[20] X.-R. Lyu,[7] G. M. Ma,[4] R. Ma,[7] S. Maccolini,[17] F. Machefert,[13] F. Maciuc,[40] I. Mackay,[61] L. R. Madhan Mohan,[53] M. M. Madurai,[51] A. Maevskiy,[41] D. Magdalinski,[35] D. Maisuzenko,[41] M. W. Majewski,[37] J. J. Malczewski,[38] S. Malde,[61] B. Malecki,[38,46] L. Malentacca,[46] A. Malinin,[41] T. Maltsev,[41] G. Manca,[29,k] G. Mancinelli,[12] C. Mancuso,[27,13,h] R. Manera Escalero,[43] D. Manuzzi,[22] D. Marangotto,[27,h] J. F. Marchand,[10] R. Marchevski,[47] U. Marconi,[22] S. Mariani,[46] C. Marin Benito,[43,46] J. Marks,[19] A. M. Marshall,[52] P. J. Marshall,[58] G. Martelli,[31,n] G. Martellotti,[33] L. Martinazzoli,[46] M. Martinelli,[28,a] D. Martinez Santos,[44] F. Martinez Vidal,[45] A. Massafferri,[2] M. Materok,[16] R. Matev,[46] A. Mathad,[48] V. Matiunin,[41] C. Matteuzzi,[66] K. R. Mattioli,[14] A. Mauri,[59] E. Maurice,[14] J. Mauricio,[43] P. Mayencourt,[47] M. Mazurek,[46] M. McCann,[59] L. Mcconnell,[20] T. H. McGrath,[60] N. T. McHugh,[57] A. McNab,[60] R. McNulty,[20] B. Meadows,[63] P. Medley,[63] G. Meier,[17] D. Melnychuk,[39] M. Merk,[35,76] A. Merli,[27,h] L. Meyer Garcia,[3] D. Miao,[5,7] H. Miao,[7] M. Mikhasenko,[73,u] D. A. Milanes,[72] A. Minotti,[28,a] E. Minucci,[66] T. Miralles,[11] S. E. Mitchell,[56] B. Mitreska,[17] D. S. Mitzel,[17] A. Modak,[55] A. Mödden,[17] R. A. Mohammed,[61] R. D. Moise,[16] S. Mokhnenko,[41] T. Mombächer,[46] M. Monk,[54,1] I. A. Monroy,[72] S. Monteil,[11] A. Morcillo Gomez,[44] G. Morello,[25] M. J. Morello,[32,d] M. P. Morgenthaler,[19] J. Moron,[37] A. B. Morris,[46] A. G. Morris,[12] R. Mountain,[66] H. Mu,[4] Z. M. Mu,[6] E. Muhammad,[54] F. Muheim,[56] M. Mulder,[75] K. Müller,[48] F. Mũnoz-Rojas,[9] R. Murta,[59] P. Naik,[58] T. Nakada,[47] R. Nandakumar,[55] T. Nanut,[46] I. Nasteva,[3] M. Needham,[56] N. Neri,[27,h] S. Neubert,[73] N. Neufeld,[46] P. Neustroev,[41] R. Newcombe,[59] J. Nicolini,[17,13] D. Nicotra,[76] E. M. Niel,[47] N. Nikitin,[41] P. Nogga,[73] N. S. Nolte,[62] C. Normand,[10,29,k] J. Novoa Fernandez,[44] G. Nowak,[63] C. Nunez,[79] H. N. Nur,[57] A. Oblakowska-Mucha,[37] V. Obraztsov,[41] T. Oeser,[16] S. Okamura,[23,46,e] R. Oldeman,[29,k] F. Oliva,[56] M. Olocco,[17] C. J. G. Onderwater,[76] R. H. O'Neil,[56] J. M. Otalora Goicochea,[3] T. Ovsiannikova,[41] P. Owen,[48] A. Oyanguren,[45] O. Ozcelik,[56] K. O. Padeken,[73] B. Pagare,[54] P. R. Pais,[19] T. Pajero,[61] A. Palano,[21] M. Palutan,[25] G. Panshin,[41] L. Paolucci,[54] A. Papanestis,[55] M. Pappagallo,[21,m] L. L. Pappalardo,[23,e] C. Pappenheimer,[63] C. Parkes,[60] B. Passalacqua,[23,e] G. Passaleva,[24] D. Passaro,[32,d] A. Pastore,[21] M. Patel,[59] J. Patoc,[61] C. Patrignani,[22,f] C. J. Pawley,[76] A. Pellegrino,[35] M. Pepe Altarelli,[25] S. Perazzini,[22] D. Pereima,[41] A. Pereiro Castro,[44] P. Perret,[11] A. Perro,[46] K. Petridis,[52] A. Petrolini,[26,g] S. Petrucci,[56] H. Pham,[66] L. Pica,[32,d] M. Piccini,[31] B. Pietrzyk,[10] G. Pietrzyk,[13] D. Pinci,[33] F. Pisani,[46] M. Pizzichemi,[28,a] V. Placinta,[40] M. Plo Casasus,[44] F. Polci,[15,46] M. Poli Lener,[25] A. Poluektov,[12] N. Polukhina,[41] I. Polyakov,[46] E. Polycarpo,[3] S. Ponce,[46] D. Popov,[7] S. Poslavskii,[41] K. Prasanth,[38] C. Prouve,[44] V. Pugatch,[50] V. Puill,[13] G. Punzi,[32,s] H. R. Qi,[4] W. Qian,[7] N. Qin,[4] S. Qu,[4] R. Quagliani,[47] R. I. Rabadan Trejo,[54] B. Rachwal,[37] J. H. Rademacker,[52] M. Rama,[32] M. Ramírez García,[79] M. Ramos Pernas,[54] M. S. Rangel,[3] F. Ratnikov,[41] G. Raven,[36] M. Rebollo De Miguel,[45] F. Redi,[46] J. Reich,[52] F. Reiss,[60] Z. Ren,[7] P. K. Resmi,[61] R. Ribatti,[32,d] G. R. Ricart,[14,80] D. Riccardi,[32,d] S. Ricciardi,[55] K. Richardson,[62] M. Richardson-Slipper,[56] K. Rinnert,[58] P. Robbe,[13] G. Robertson,[57] E. Rodrigues,[58,46] E. Rodriguez Fernandez,[44] J. A. Rodriguez Lopez,[72] E. Rodriguez Rodriguez,[44] A. Rogovskiy,[55] D. L. Rolf,[46] A. Rollings,[61] P. Roloff,[46] V. Romanovskiy,[41] M. Romero Lamas,[44] A. Romero Vidal,[44] G. Romolini,[23] F. Ronchetti,[47] M. Rotondo,[25] S. R. Roy,[19] M. S. Rudolph,[66] T. Ruf,[46] M. Ruiz Diaz,[19] R. A. Ruiz Fernandez,[44] J. Ruiz Vidal,[78,v] A. Ryzhikov,[41] J. Ryzka,[37] J. J. Saborido Silva,[44] R. Sadek,[14] N. Sagidova,[41] N. Sahoo,[51] B. Saitta,[29,k] M. Salomoni,[28,a] C. Sanchez Gras,[35] I. Sanderswood,[45] R. Santacesaria,[33] C. Santamarina Rios,[44] M. Santimaria,[25] L. Santoro,[2] E. Santovetti,[34] A. Saputi,[23,46] D. Saranin,[41] G. Sarpis,[56] M. Sarpis,[73] A. Sarti,[33] C. Satriano,[33,w] A. Satta,[34] M. Saur,[6] D. Savrina,[41] H. Sazak,[11] L. G. Scantlebury Smead,[61] A. Scarabotto,[15] S. Schael,[16] S. Scherl,[58] A. M. Schertz,[74] M. Schiller,[57] H. Schindler,[46] M. Schmelling,[18] B. Schmidt,[46] S. Schmitt,[16] H. Schmitz,[73] O. Schneider,[47] A. Schopper,[46] N. Schulte,[17] S. Schulte,[47] M. H. Schune,[13] R. Schwemmer,[46] G. Schwering,[16] B. Sciascia,[25] A. Sciuccati,[46] S. Sellam,[44] A. Semennikov,[41] M. Senghi Soares,[36] A. Sergi,[26,g] N. Serra,[48,46] L. Sestini,[30] A. Seuthe,[17] Y. Shang,[6] D. M. Shangase,[79] M. Shapkin,[41] I. Shchemerov,[41] L. Shchutska,[47] T. Shears,[58] L. Shekhtman,[41] Z. Shen,[6] S. Sheng,[5,7] V. Shevchenko,[41] B. Shi,[7] E. B. Shields,[28,a] Y. Shimizu,[13] E. Shmanin,[41] R. Shorkin,[41] J. D. Shupperd,[66] R. Silva Coutinho,[66] G. Simi,[30] S. Simone,[21,m] N. Skidmore,[60] R. Skuza,[19] T. Skwarnicki,[66] M. W. Slater,[51] J. C. Smallwood,[61] E. Smith,[62] K. Smith,[65] M. Smith,[59] A. Snoch,[35] L. Soares Lavra,[56] M. D. Sokoloff,[63] F. J. P. Soler,[57] A. Solomin,[41,52] A. Solovev,[41] I. Solovyev,[41] R. Song,[1] Y. Song,[47] Y. Song,[4] Y. S. Song,[6] F. L. Souza De Almeida,[66] B. Souza De Paula,[3] E. Spadaro Norella,[27,h] E. Spedicato,[22] J. G. Speer,[17] E. Spiridenkov,[41] P. Spradlin,[57] V. Sriskaran,[46] F. Stagni,[46] M. Stahl,[46] S. Stahl,[46] S. Stanislaus,[61] E. N. Stein,[46] O. Steinkamp,[48] O. Stenyakin,[41] H. Stevens,[17] D. Strekalina,[41] Y. Su,[7] F. Suljik,[61] J. Sun,[29] L. Sun,[71] Y. Sun,[64] P. N. Swallow,[51]

K. Swientek,[37] F. Swystun,[54] A. Szabelski,[39] T. Szumlak,[37] M. Szymanski,[46] Y. Tan,[4] S. Taneja,[60] M. D. Tat,[61] A. Terentev,[48] F. Terzuoli,[32,x] F. Teubert,[46] E. Thomas,[46] D. J. D. Thompson,[51] H. Tilquin,[59] V. Tisserand,[11] S. T'Jampens,[10] M. Tobin,[5] L. Tomassetti,[23,e] G. Tonani,[27,h] X. Tong,[6] D. Torres Machado,[2] L. Toscano,[17] D. Y. Tou,[4] C. Trippl,[42] G. Tuci,[19] N. Tuning,[35] L. H. Uecker,[19] A. Ukleja,[37] D. J. Unverzagt,[19] E. Ursov,[41] A. Usachov,[36] A. Ustyuzhanin,[41] U. Uwer,[19] V. Vagnoni,[22] A. Valassi,[46] G. Valenti,[22] N. Valls Canudas,[42] H. Van Hecke,[65] E. van Herwijnen,[59] C. B. Van Hulse,[44,y] R. Van Laak,[47] M. van Veghel,[35] R. Vazquez Gomez,[43] P. Vazquez Regueiro,[44] C. Vázquez Sierra,[44] S. Vecchi,[23] J. J. Velthuis,[52] M. Veltri,[24,z] A. Venkateswaran,[47] M. Vesterinen,[54] D. Vieira,[63] M. Vieites Diaz,[46] X. Vilasis-Cardona,[42] E. Vilella Figueras,[58] A. Villa,[22] P. Vincent,[15] F. C. Volle,[13] D. vom Bruch,[12] V. Vorobyev,[41] N. Voropaev,[41] K. Vos,[76] G. Vouters,[10] C. Vrahas,[56] J. Walsh,[32] E. J. Walton,[1] G. Wan,[6] C. Wang,[19] G. Wang,[8] J. Wang,[6] J. Wang,[5] J. Wang,[4] J. Wang,[71] M. Wang,[27] N. W. Wang,[7] R. Wang,[52] X. Wang,[69] X. W. Wang,[59] Y. Wang,[8] Z. Wang,[13] Z. Wang,[4] Z. Wang,[7] J. A. Ward,[54,1] N. K. Watson,[51] D. Websdale,[59] Y. Wei,[6] B. D. C. Westhenry,[52] D. J. White,[60] M. Whitehead,[57] A. R. Wiederhold,[54] D. Wiedner,[17] G. Wilkinson,[61] M. K. Wilkinson,[63] M. Williams,[62] M. R. J. Williams,[56] R. Williams,[53] F. F. Wilson,[55] W. Wislicki,[39] M. Witek,[38] L. Witola,[19] C. P. Wong,[65] G. Wormser,[13] S. A. Wotton,[53] H. Wu,[66] J. Wu,[8] Y. Wu,[6] K. Wyllie,[46] S. Xian,[69] Z. Xiang,[5] Y. Xie,[8] A. Xu,[32] J. Xu,[7] L. Xu,[4] L. Xu,[4] M. Xu,[54] Z. Xu,[11] Z. Xu,[7] Z. Xu,[5] D. Yang,[4] S. Yang,[7] X. Yang,[6] Y. Yang,[26,g] Z. Yang,[6] Z. Yang,[64] V. Yeroshenko,[13] H. Yeung,[60] H. Yin,[8] C. Y. Yu,[6] J. Yu,[68] X. Yuan,[5] E. Zaffaroni,[47] M. Zavertyaev,[18] M. Zdybal,[38] M. Zeng,[4] C. Zhang,[6] D. Zhang,[8] J. Zhang,[7] L. Zhang,[4] S. Zhang,[68] S. Zhang,[6] Y. Zhang,[6] Y. Zhang,[61] Y. Z. Zhang,[4] Y. Zhao,[19] A. Zharkova,[41] A. Zhelezov,[19] X. Z. Zheng,[4] Y. Zheng,[7] T. Zhou,[6] X. Zhou,[8] Y. Zhou,[7] V. Zhovkovska,[54] L. Z. Zhu,[7] X. Zhu,[4] X. Zhu,[8] Z. Zhu,[7] V. Zhukov,[16,41] J. Zhuo,[45] Q. Zou,[5,7] D. Zuliani,[30] and G. Zunica[60]

(LHCb Collaboration)

[1]*School of Physics and Astronomy, Monash University, Melbourne, Australia*
[2]*Centro Brasileiro de Pesquisas Físicas (CBPF), Rio de Janeiro, Brazil*
[3]*Universidade Federal do Rio de Janeiro (UFRJ), Rio de Janeiro, Brazil*
[4]*Center for High Energy Physics, Tsinghua University, Beijing, China*
[5]*Institute Of High Energy Physics (IHEP), Beijing, China*
[6]*School of Physics State Key Laboratory of Nuclear Physics and Technology, Peking University, Beijing, China*
[7]*University of Chinese Academy of Sciences, Beijing, China*
[8]*Institute of Particle Physics, Central China Normal University, Wuhan, Hubei, China*
[9]*Consejo Nacional de Rectores (CONARE), San Jose, Costa Rica*
[10]*Université Savoie Mont Blanc, CNRS, IN2P3-LAPP, Annecy, France*
[11]*Université Clermont Auvergne, CNRS/IN2P3, LPC, Clermont-Ferrand, France*
[12]*Aix Marseille Univ, CNRS/IN2P3, CPPM, Marseille, France*
[13]*Université Paris-Saclay, CNRS/IN2P3, IJCLab, Orsay, France*
[14]*Laboratoire Leprince-Ringuet, CNRS/IN2P3, Ecole Polytechnique, Institut Polytechnique de Paris, Palaiseau, France*
[15]*LPNHE, Sorbonne Université, Paris Diderot Sorbonne Paris Cité, CNRS/IN2P3, Paris, France*
[16]*I. Physikalisches Institut, RWTH Aachen University, Aachen, Germany*
[17]*Fakultät Physik, Technische Universität Dortmund, Dortmund, Germany*
[18]*Max-Planck-Institut für Kernphysik (MPIK), Heidelberg, Germany*
[19]*Physikalisches Institut, Ruprecht-Karls-Universität Heidelberg, Heidelberg, Germany*
[20]*School of Physics, University College Dublin, Dublin, Ireland*
[21]*INFN Sezione di Bari, Bari, Italy*
[22]*INFN Sezione di Bologna, Bologna, Italy*
[23]*INFN Sezione di Ferrara, Ferrara, Italy*
[24]*INFN Sezione di Firenze, Firenze, Italy*
[25]*INFN Laboratori Nazionali di Frascati, Frascati, Italy*
[26]*INFN Sezione di Genova, Genova, Italy*
[27]*INFN Sezione di Milano, Milano, Italy*
[28]*INFN Sezione di Milano-Bicocca, Milano, Italy*
[29]*INFN Sezione di Cagliari, Monserrato, Italy*
[30]*Università degli Studi di Padova, Università e INFN, Padova, Padova, Italy*
[31]*INFN Sezione di Perugia, Perugia, Italy*
[32]*INFN Sezione di Pisa, Pisa, Italy*
[33]*INFN Sezione di Roma La Sapienza, Roma, Italy*
[34]*INFN Sezione di Roma Tor Vergata, Roma, Italy*

[35]*Nikhef National Institute for Subatomic Physics, Amsterdam, Netherlands*
[36]*Nikhef National Institute for Subatomic Physics and VU University Amsterdam, Amsterdam, Netherlands*
[37]*AGH - University of Science and Technology, Faculty of Physics and Applied Computer Science, Kraków, Poland*
[38]*Henryk Niewodniczanski Institute of Nuclear Physics Polish Academy of Sciences, Kraków, Poland*
[39]*National Center for Nuclear Research (NCBJ), Warsaw, Poland*
[40]*Horia Hulubei National Institute of Physics and Nuclear Engineering, Bucharest-Magurele, Romania*
[41]*Affiliated with an institute covered by a cooperation agreement with CERN*
[42]*DS4DS, La Salle, Universitat Ramon Llull, Barcelona, Spain*
[43]*ICCUB, Universitat de Barcelona, Barcelona, Spain*
[44]*Instituto Galego de Física de Altas Enerxías (IGFAE), Universidade de Santiago de Compostela, Santiago de Compostela, Spain*
[45]*Instituto de Fisica Corpuscular, Centro Mixto Universidad de Valencia - CSIC, Valencia, Spain*
[46]*European Organization for Nuclear Research (CERN), Geneva, Switzerland*
[47]*Institute of Physics, Ecole Polytechnique Fédérale de Lausanne (EPFL), Lausanne, Switzerland*
[48]*Physik-Institut, Universität Zürich, Zürich, Switzerland*
[49]*NSC Kharkiv Institute of Physics and Technology (NSC KIPT), Kharkiv, Ukraine*
[50]*Institute for Nuclear Research of the National Academy of Sciences (KINR), Kyiv, Ukraine*
[51]*University of Birmingham, Birmingham, United Kingdom*
[52]*H.H. Wills Physics Laboratory, University of Bristol, Bristol, United Kingdom*
[53]*Cavendish Laboratory, University of Cambridge, Cambridge, United Kingdom*
[54]*Department of Physics, University of Warwick, Coventry, United Kingdom*
[55]*STFC Rutherford Appleton Laboratory, Didcot, United Kingdom*
[56]*School of Physics and Astronomy, University of Edinburgh, Edinburgh, United Kingdom*
[57]*School of Physics and Astronomy, University of Glasgow, Glasgow, United Kingdom*
[58]*Oliver Lodge Laboratory, University of Liverpool, Liverpool, United Kingdom*
[59]*Imperial College London, London, United Kingdom*
[60]*Department of Physics and Astronomy, University of Manchester, Manchester, United Kingdom*
[61]*Department of Physics, University of Oxford, Oxford, United Kingdom*
[62]*Massachusetts Institute of Technology, Cambridge, Massachusetts, USA*
[63]*University of Cincinnati, Cincinnati, Ohio, USA*
[64]*University of Maryland, College Park, Maryland, USA*
[65]*Los Alamos National Laboratory (LANL), Los Alamos, New Mexico, USA*
[66]*Syracuse University, Syracuse, New York, USA*
[67]*Pontifícia Universidade Católica do Rio de Janeiro (PUC-Rio), Rio de Janeiro, Brazil, associated with 3*
[68]*School of Physics and Electronics, Hunan University, Changsha City, China, associated with 8*
[69]*Guangdong Provincial Key Laboratory of Nuclear Science, Guangdong-Hong Kong Joint Laboratory of Quantum Matter, Institute of Quantum Matter, South China Normal University, Guangzhou, China, associated with 4*
[70]*Lanzhou University, Lanzhou, China, associated with 5*
[71]*School of Physics and Technology, Wuhan University, Wuhan, China, associated with 4*
[72]*Departamento de Fisica, Universidad Nacional de Colombia, Bogota, Colombia, associated with 15*
[73]*Universität Bonn - Helmholtz-Institut für Strahlen und Kernphysik, Bonn, Germany, associated with 19*
[74]*Eotvos Lorand University, Budapest, Hungary, associated with 46*
[75]*Van Swinderen Institute, University of Groningen, Groningen, Netherlands, associated with 35*
[76]*Universiteit Maastricht, Maastricht, Netherlands, associated with 35*
[77]*Tadeusz Kosciuszko Cracow University of Technology, Cracow, Poland, associated with 38*
[78]*Department of Physics and Astronomy, Uppsala University, Uppsala, Sweden, associated with 57*
[79]*University of Michigan, Ann Arbor, Michigan, USA, associated with 66*
[80]*Departement de Physique Nucleaire (SPhN), Gif-Sur-Yvette, France*

[a]Università di Milano Bicocca, Milano, Italy.
[b]Università di Roma Tor Vergata, Roma, Italy.
[c]Università di Firenze, Firenze, Italy.
[d]Scuola Normale Superiore, Pisa, Italy.
[e]Università di Ferrara, Ferrara, Italy.
[f]Università di Bologna, Bologna, Italy.
[g]Università di Genova, Genova, Italy.
[h]Università degli Studi di Milano, Milano, Italy.
[i]Universidade da Coruña, Coruña, Spain.
[j]Universidad Nacional Autónoma de Honduras, Tegucigalpa, Honduras.
[k]Università di Cagliari, Cagliari, Italy.

[l]Centro Federal de Educacão Tecnológica Celso Suckow da Fonseca, Rio De Janeiro, Brazil.
[m]Università di Bari, Bari, Italy.
[n]Università di Perugia, Perugia, Italy.
[o]LIP6, Sorbonne Universite, Paris, France.
[p]Universidade de Brasília, Brasília, Brazil.
[q]Deceased.
[r]Hangzhou Institute for Advanced Study, UCAS, Hangzhou, China.
[s]Università di Pisa, Pisa, Italy.
[t]Università di Padova, Padova, Italy.
[u]Excellence Cluster ORIGINS, Munich, Germany.
[v]Department of Physics/Division of Particle Physics, Lund, Sweden.
[w]Università della Basilicata, Potenza, Italy.
[x]Università di Siena, Siena, Italy.
[y]Universidad de Alcalá, Alcalá de Henares, Spain.
[z]Università di Urbino, Urbino, Italy.